Supporting Information

for

Dynamic Covalent Switching between a 1,1'-Ruthenocene Macrocycle and a Ruthenocenophane through a Transimination Reaction

Max Roemer, Gilles Frison, Han Vinh Huynh

Correspondence to: max.roemer@nus.edu.sg, chmhhv@nus.edu.sg

1. Syntheses

General

The reactions were conducted under high-purity argon atmospheres unless stated otherwise. THF and hexanes were dried from sodium/benzophenone. TMEDA was dried from sodium. Chloroform was distilled from calcium hydride. Chloroform-*d* was

either stored over K_2CO_3 or distilled from CaH_2. Ruthenocene was purchased from AK Scientific. **[PdBr$_2$(^{i}Pr$_2$-bimy)]$_2$** was prepared according to the literature.[1] Syringe filtrations were conducted with syringe filters equipped with a hydrophobic PTFE membrane (pore size: 0.22 µm). NMR spectra were recorded on Bruker AV500, AVNEO500 (2D), and AV400 spectrometers and referenced versus residual solvent signals.[2] Low-resolution mass spectra were recorded on a Thermo Scientific LCQ Fleet LCMS system in electrospray positive mode (ESI+). High-resolution mass spectra were recorded on an Agilent 6546 quadrupole time of flight LC mass spectrometer in electrospray positive mode (ESI+).

1.1. Starting Materials

We employed a modified literature protocol to synthesise 1,1'-diformylruthenocene (**1**).[3, 4] In analogy to the preparation of the 1,1'-iodoferrocene by lithiation of ferrocene in hexanes with *n*-butyllithium/TMEDA and subsequent reaction with iodine in hexanes/THF,[5] 1,1'-diformyl ruthenocene can be obtained in good yield by lithiation of ruthenocene with *n*-butyllithium/TMEDA and subsequent reaction with DMF in hexanes/THF, followed by acidic work-up.

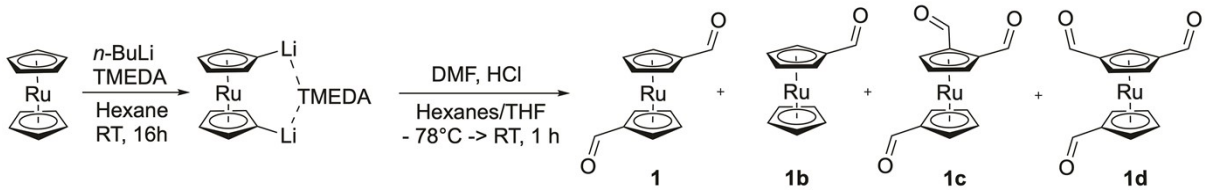

Scheme S1. Synthesis of 1,1'-diformylruthenocene (**1**).

As reported earlier by others,[3, 4] the reaction yields apart from (mono) formylruthenocene (**1d**) also higher-order formylruthenocenes (**1c** and **1d**) as by-products, owing to the increased reactivity towards organolithium reagents relative to

ferrocene. These could be separated chromatographically from the target compound **1**.

1,1'-Diformylruthenocene (**1**)**.** An oven-dried Schlenk flask equipped with a magnetic stirring bar was charged with ruthenocene (2.0 g, 8.6 mmol) and hexanes (100 mL). TMEDA (3.2 mL, 21.6 mmol) was added, and the mixture was stirred at room temperature for five min, yielding a partial solution with some ruthenocene remaining undissolved. *n*-Butyllithium (2.0 M in cyclohexane) was added with a syringe (10.8 mL, 21.6 mmol), and the mixture was stirred overnight. A thick whitish precipitation formed over the course of the reaction. The solids were agitated, the suspension was cooled to -78 °C, and THF (100 mL) was added slowly with a syringe. An excess of DMF (6.4 mL, 3 equiv.) was added to the suspension with a syringe, and the mixture was stirred and allowed to warm to room temperature. Aqueous hydrochloric acid (10 %, 40 mL) was added, and the solution was extracted with dichloromethane (2 x 150 mL). The organic layers were combined and dried over sodium sulfate. Solvent evaporation and drying under high vacuum yielded a crystalline solid, which was further purified by column chromatography on silica gel using hexanes/ethyl acetate (2:1) as eluent. The first fraction contained unreacted ruthenocene; the second fraction contained **1b**, the third fraction contained the target product (**1**), and the fourth fraction contained a mixture of **1** and higher-order ruthenocene carboxaldehydes, presumably the 1,1',2'- and 1,1',3'-ruthenocene carboxaldehydes. Solvent evaporation and drying under high vacuum from the third fraction yielded **1** (1.224 g, 4.3 mmol, 49%) as dark yellow-brownish crystalline material. The NMR spectroscopic data of **1** were consistent with the literature.[4]

1.2. Synthesis of the Macrocycle 2a

Synthesis in Solution:

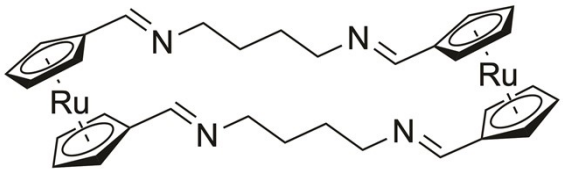

2a

Compound **1** (300 mg, 1.0 mmol) was dissolved in methanol (45 mL), followed by the addition of 1,4-diaminobutane (460 mg, 5.2 mmol). The mixture was stirred at room temperature for three hours. Subsequently, the solvent was removed *in vacuo,* and the crude product was dried under high vacuum. This partially removed the excess 1,4-diaminobutane. The remaining oily solids were dissolved in dichloromethane and recrystallised twice at - 25°C, yielding a light-yellow crystalline material (244 mg, 0.7 mmol, 69%). Different types of single crystals were obtained upon recrystallisation from dichloromethane at - 25°C. The vast majority contained dichloromethane as solvate (light yellow needles), but a minor amount contained no solvate (colourless platelets) as determined by single crystal X-ray diffraction (Figure S1).

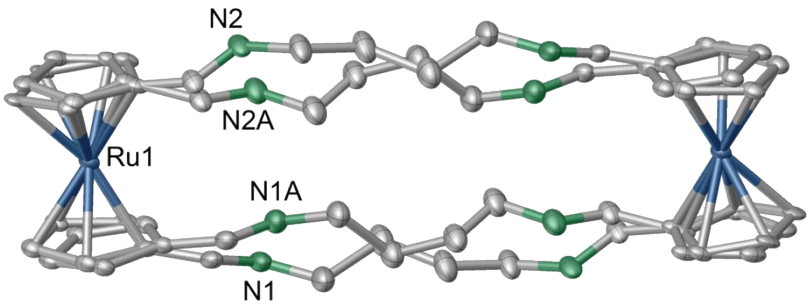

Figure S1. Molecular structure of macrocycle **2a**, crystallised without a solvate molecule. All atoms, except the Ru atoms, are disordered into two positions with an occupancy ratio of 63:37. Ellipsoids are drawn at a 50% probability level.

We also obtained a molecular structure of the compound with water as a solvate (Figure S2).

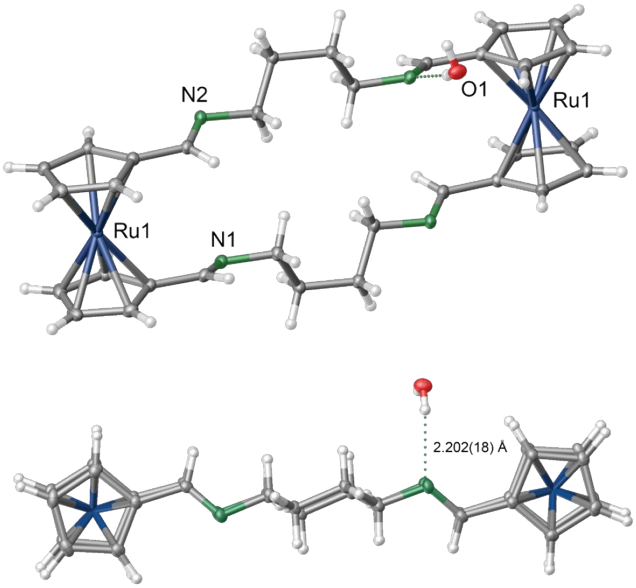

Figure S2. Molecular structure of macrocycle **2a**, containing a water solvate molecule. Ellipsoids are drawn at a 50% probability level.

Mechanochemical Synthesis:

On air, compound **1** (150 mg, 0.5 mmol) and 1,4-diaminobutane (184 mg, 2.1 mmol) were mixed in a standard 4 mL screw cap glass vial. The mixture was agitated and ground with a glass rod. Grinding was conducted in a circular motion, ensuring that no reactants accumulated on the vial's glass wall. This was achieved by periodically pushing the oily mixture from the walls down to the bottom. We monitored the reaction by ^{1}H NMR spectroscopy. After 15 minutes of grinding, completion was already >95% based on the integration of ^{1}H NMR resonances of the product, starting material, and intermediates. Two singlets of low intensity, in the vicinity of 9.7 ppm, were still visible, originating from the formyl group of unreacted **1** and likely a mono-formyl intermediate. These signals disappeared entirely after an additional 15 min of grinding, indicating a quantitative reaction to **2a**. We found that the excess of 1,4-diaminobutane was necessary to achieve quantitative conversion on the scales used, within the given grinding timeframe. Removal of most of the excess 1,4-diaminobutane was achieved

under high vacuum (0.010 mbar) at elevated temperature (120°C), yielding a hard, light-brown, glass-like solid as the residue. This residue was dissolved in dichloromethane and re-crystallised at -25 °C to yield a pale-yellow crystalline powder (127 mg, 0.19 mmol, 72%).^{1}H NMR (500 MHz, $CDCl_3$) δ 7.86 (s, 4H, C*H*N), 4.99 (pst, *J* = 1.8 Hz, 8H, Cp-*H*^{2}), 4.68 (pst, *J* = 1.8 Hz, 8H, Cp-*H*^{3}), 3.40 (m, 4H, CHNC*H*$_2$), 1.66 (m, 4H, CHNCH$_2$C*H*$_2$) ppm. ^{13}C NMR (101 MHz, $CDCl_3$) δ 159.1 (*C*HN), 86.5 (ipso-*C*), 72.6 (Cp, *C*$_3$), 71.6 (Cp, *C*$_2$), 61.6 (CHN*C*H$_2$CH$_2$), 28.7 (CHNCH$_2$*C*H$_2$) ppm. MS(ESI+, from mixture with **2b**): 680 [M(**2a**) + H]$^+$ (100%), 341 [M(**2b**) + H]$^+$ (90%). HRMS (ESI+): Calcd for $C_{32}H_{37}N_4[^{102}Ru]_2$: 681.1118; found: 681.1113. Elemental analysis: Calcd for $C_{32}H_{36}N_4Ru_2$: C, 56.6; H, 5.35; N, 8.25; Calcd for $C_{32}H_{36}N_4Ru_2 \cdot H_2O$: C, 55.2; H, 5.5; N, 8.0; Found: C, 55.5; H, 5.2; N, 8.6. As confirmed by single crystal X-ray diffraction, compound **2a** can trap water in the crystal (Figure S2). Therefore, the sample may contain water molecules, explaining the deviation of the detected C value from the theoretical value.

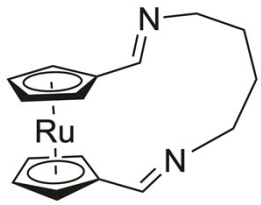

2b

Compound **2b** was synthesised by dissolving **2a** in chloroform-*d* and heating the mixture. The title compound was characterised only in solution from a mixture with **2a**. Assignments of the ^{1}H and ^{13}C NMR resonances were conducted with the aid of 2D NMR experiments (Figures S3-S9). ^{1}H NMR (500 MHz, $CDCl_3$) δ 7.78 (m, 2H, C*H*N), 5.07 (pst, *J* = 1.7 Hz, 4H, Cp-*H*^{2}), 4.69 (pst, *J* = 1.6 Hz, 4H, Cp-*H*^{3}), 3.46 (m, 4H, CHNC*H*$_2$), 1.81 (m, 4H, CHNCH$_2$C*H*$_2$). ^{13}C NMR (101 MHz, $CDCl_3$) δ 158.6 (*C*HN), 86.1 (ipso-*C*), 72.9 (Cp, *C*$_3$), 71.56 (Cp, *C*$_2$), 59.1 (CHN*C*H$_2$CH$_2$), 28.0 (CHNCH$_2$*C*H$_2$) ppm. MS(ESI+, from mixture with **2a**): 680 [M(**2a**) + H]$^+$ (100%), 341 [M(**2b**) + H]$^+$ (90%). %). HRMS (ESI+): Calcd for $C_{16}H_{19}N_2[^{102}Ru]$: 341.0591; found: 341.0592.

1.3. 2D NMR Spectra of the Mixture of 2a and 2b

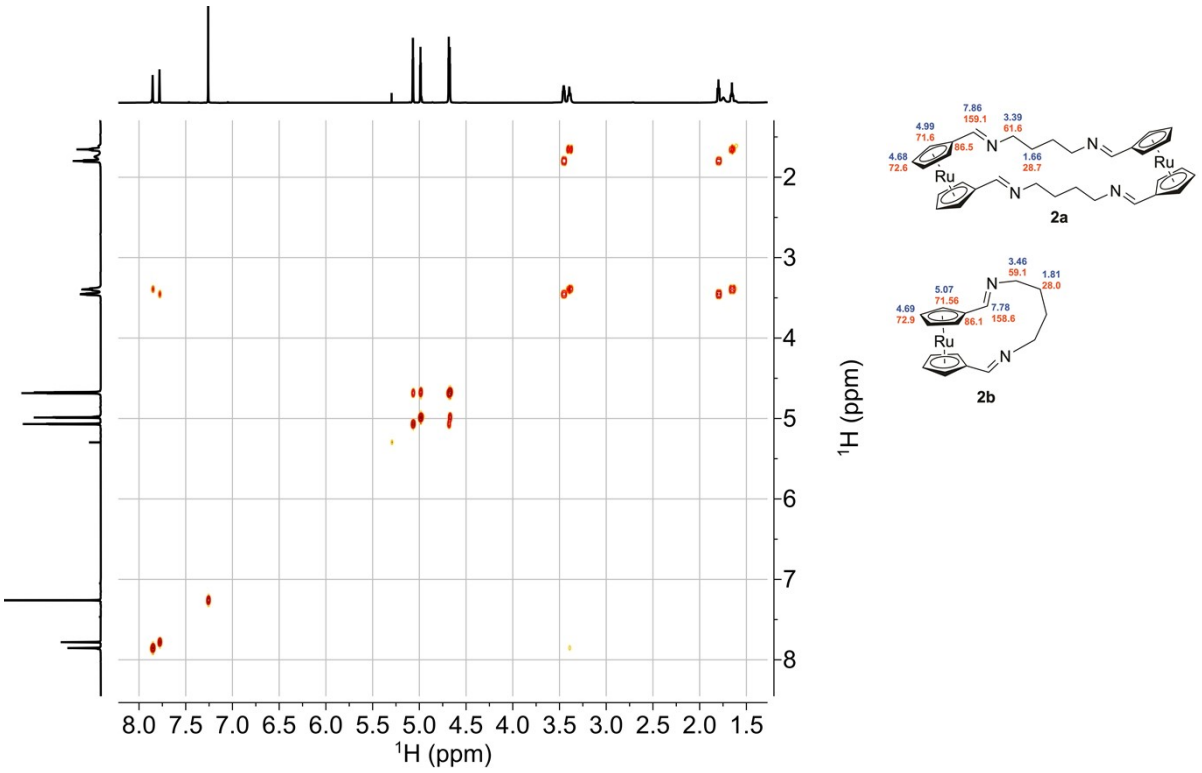

Figure S3. 2D COSY NMR spectrum of the mixture of **2a** and **2b**.

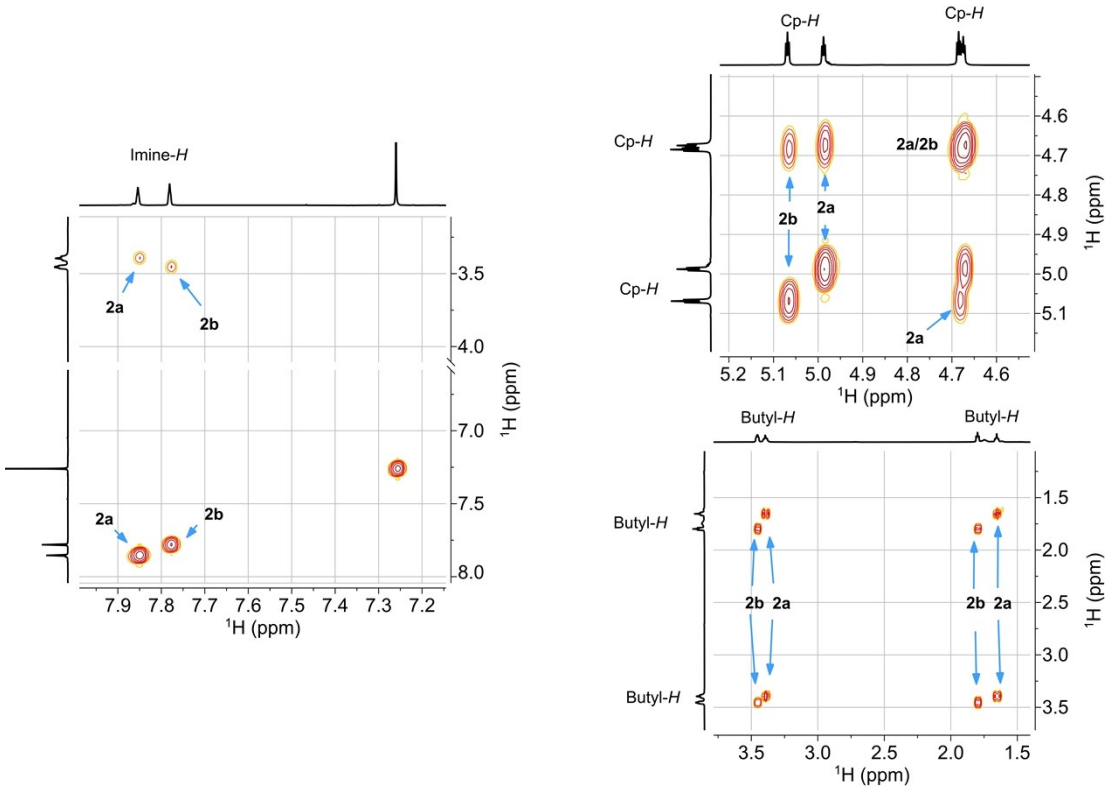

Figure S4. Magnified areas of the 2D COSY NMR spectrum of the mixture of **2a**/**2b**.

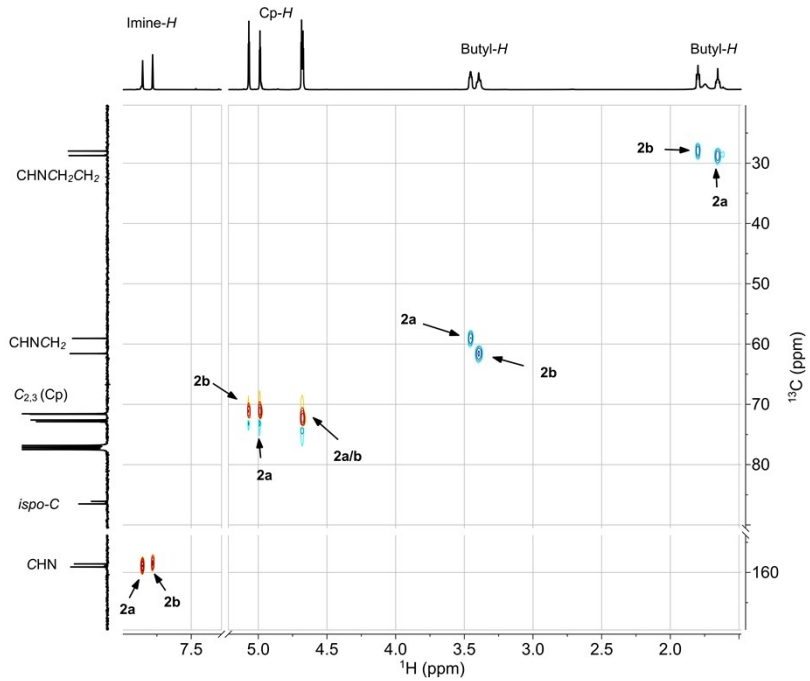

Figure S5. 2D HSQC NMR spectrum of the mixture of **2a** and **2b**.

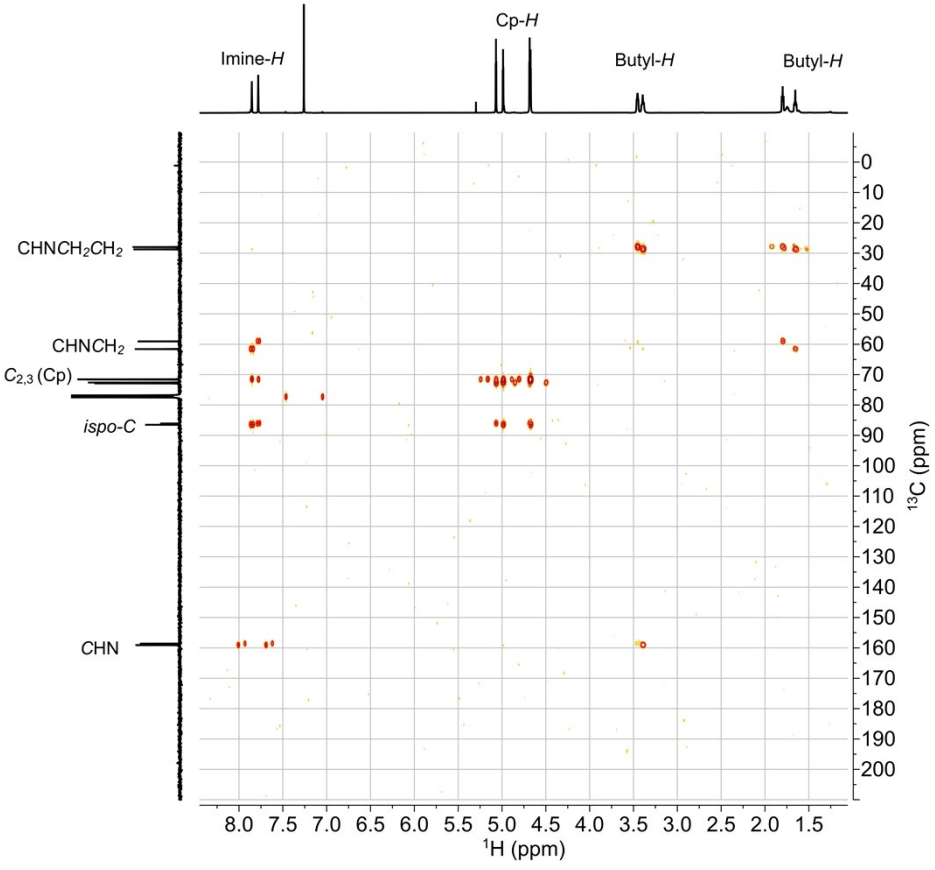

Figure S6. 2D HMBC NMR spectrum of the mixture of **2a** and **2b**.

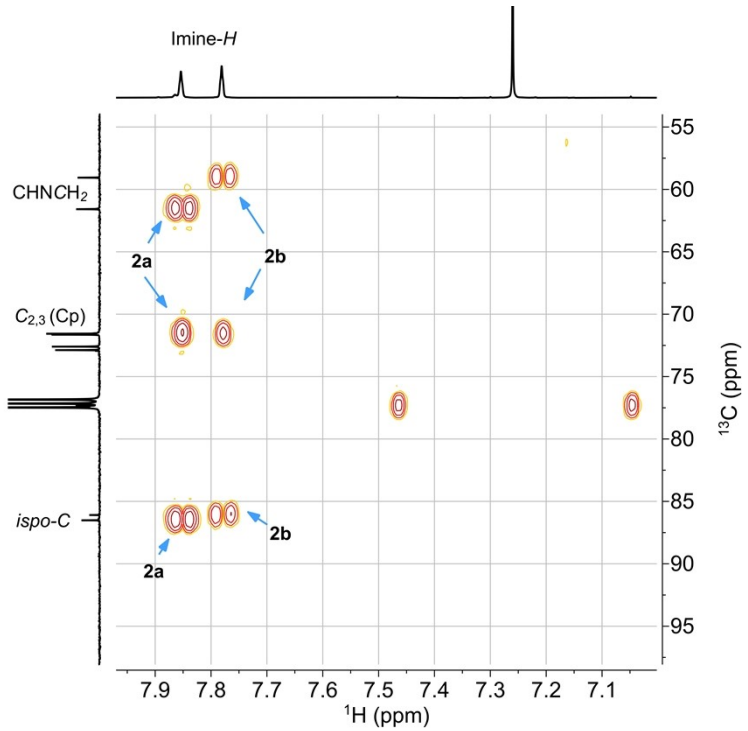

Figure S7. Magnified area of the 2D HMBC NMR spectrum of the mixture of **2a** and **2b**.

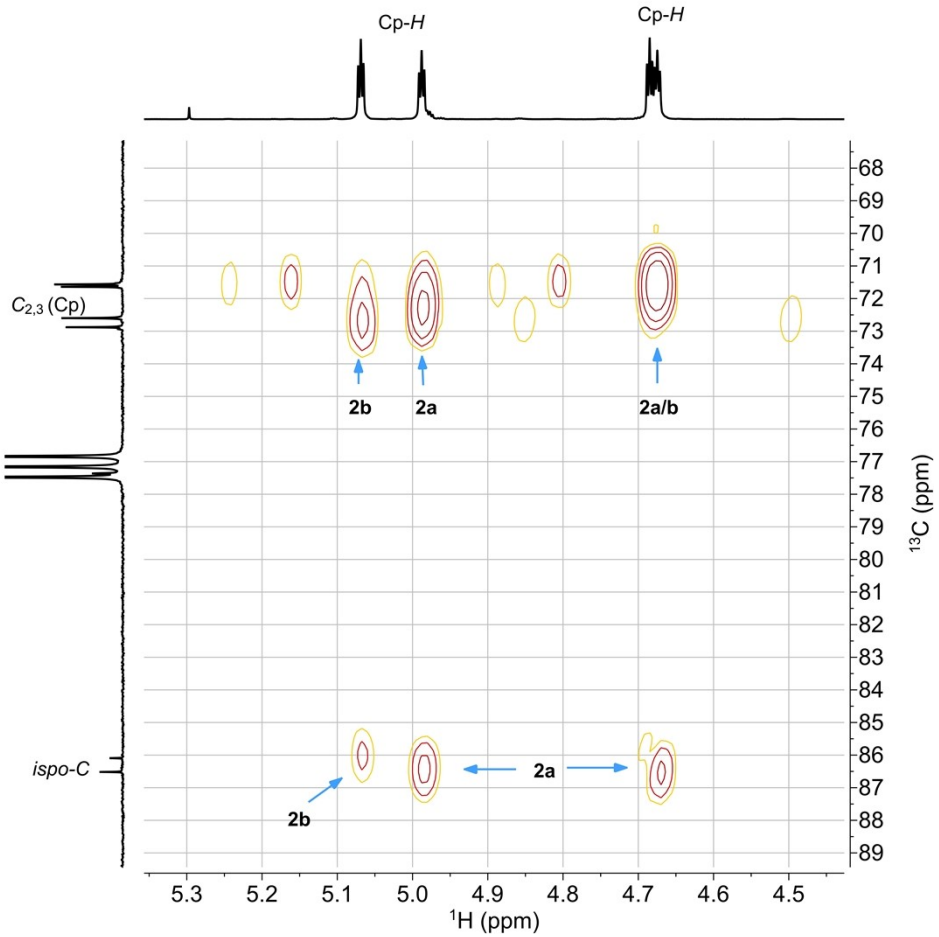

Figure S8. Magnified area of the 2D HMBC NMR spectrum of the mixture of **2a** and **2b**.

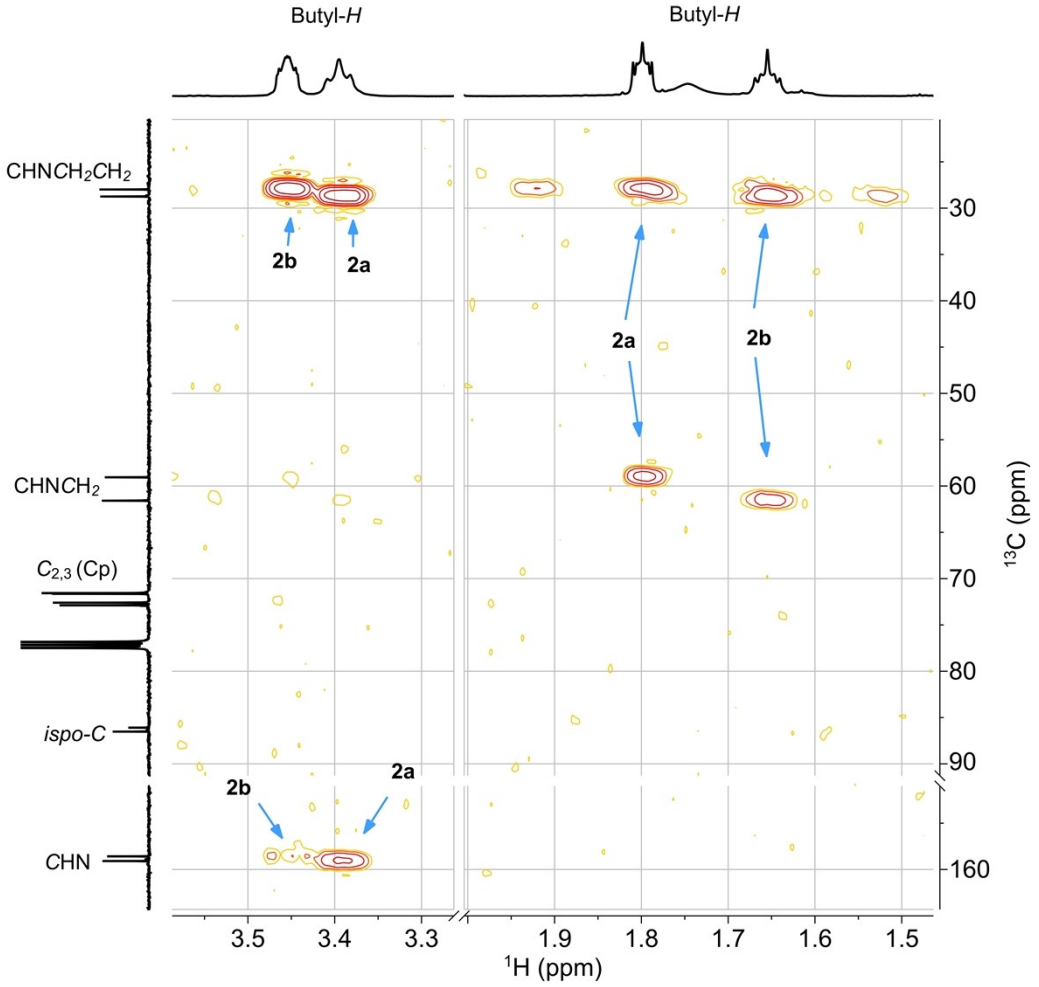

Figure S9. Magnified area of the 2D HMBC NMR spectrum of the mixture of **2a**/**2b**.

To further assign both components of the mixture, ^{1}H diffusion-ordered spectroscopy (DOSY) studies were carried out. DOSY distinguishes between the size of the components, as both components have different diffusion coefficients. We prepared a solution of **2a** in $CDCl_3$ (3 mg / mL) and recorded a ^{1}H NMR spectrum (Figure S10), followed by a ^{1}H DOSY NMR spectrum (Figure S11). The DOSY clearly shows one major component and a minor component, which is smaller and has a higher diffusion coefficient. The chemical shifts of the major component belong to **2a** and the ones of the minor component to **2b**. We have repeated the same experiment after heating the mixture for 2h at 50 °C (Figure S12 and S13). The minor component has gained significant intensity, indicating transformation of **2a** -> 2 **2b**.

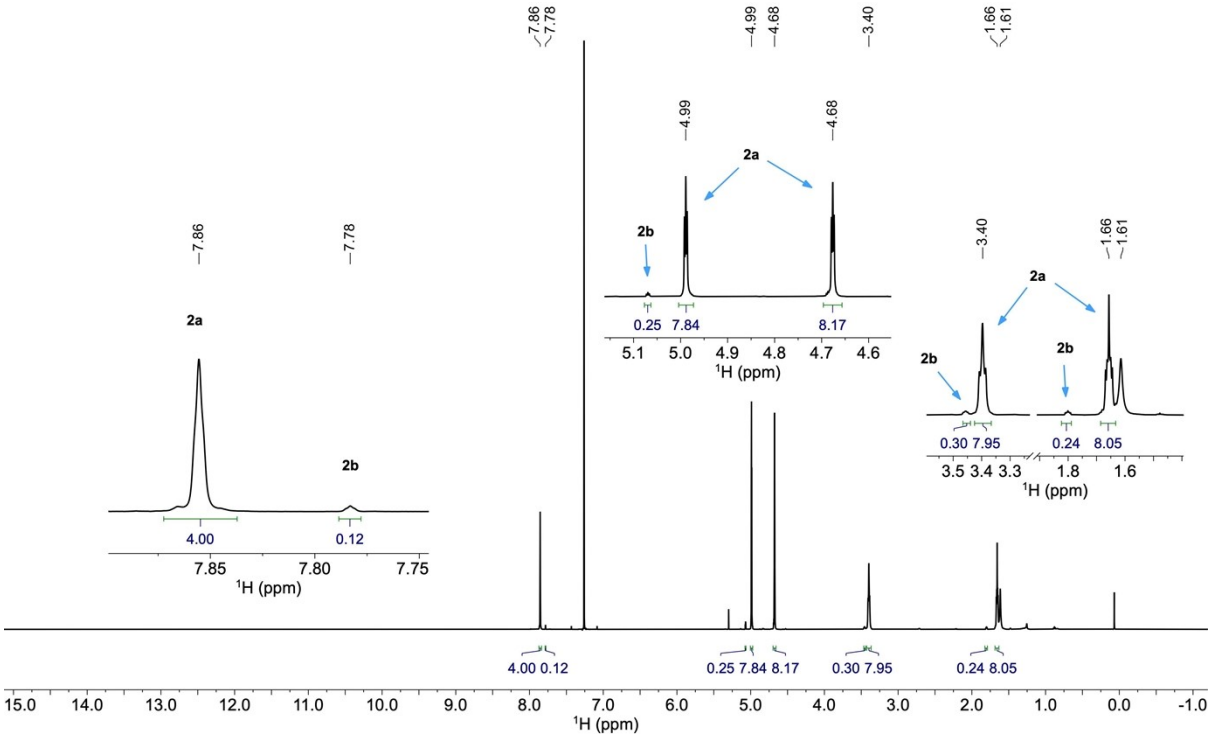

Figure S10. ^{1}H NMR spectrum of the mixture of **2a** and **2b**, before heating.

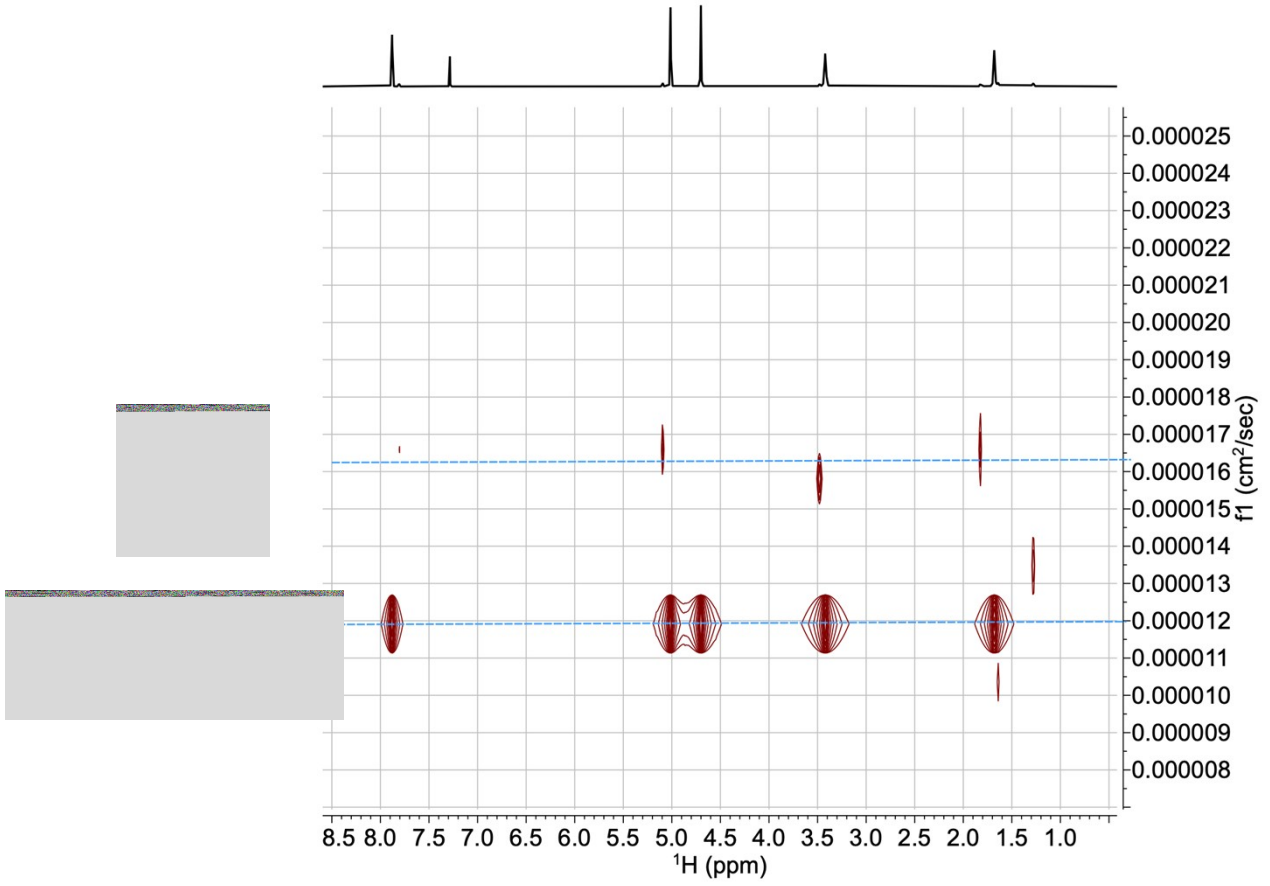

Figure S11. ^{1}H DOSY NMR spectrum (600 MHz) of the mixture of **2a** and **2b**, before heating.

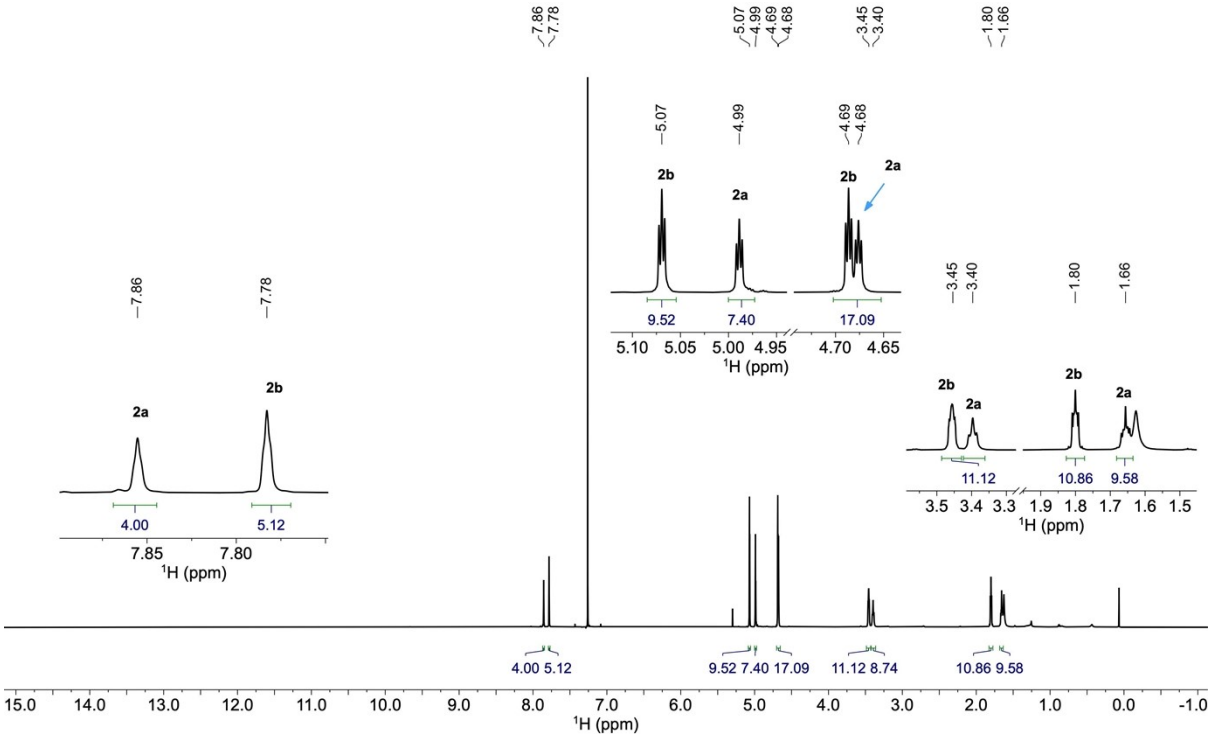

Figure S12. ^{1}H NMR spectrum of the mixture of **2a** and **2b**, after heating for 2h to 50 °C.

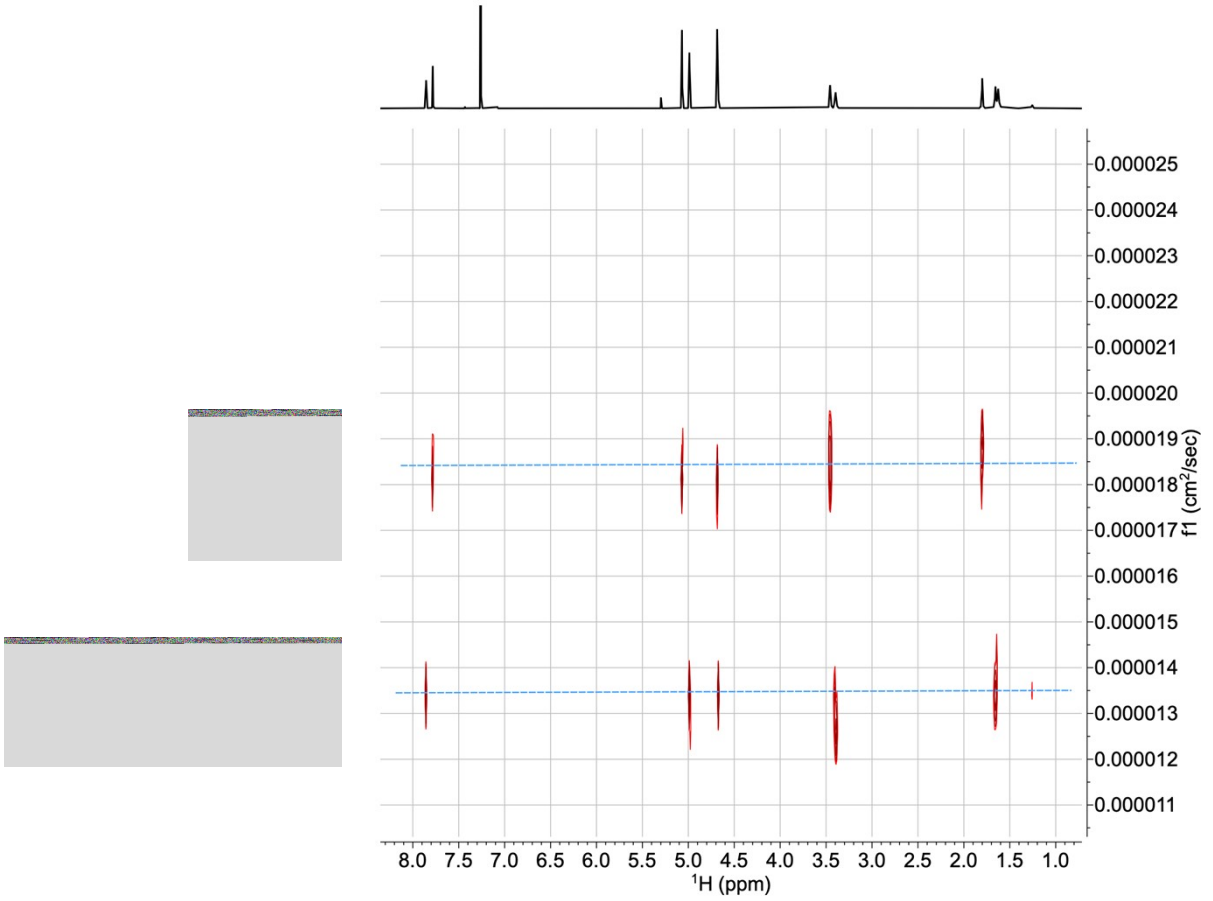

Figure S13. ^{1}H DOSY NMR spectrum (600 MHz) of the mixture of **2a** and **2b**, after heating for 2h to 50 °C.

To further assess switching fatigue, we run one cycle with 1,3,5-trimethoxybenzene (TMB) as an internal standard. We prepared a solution of **2a** in $CDCl_3$ (3 mg / mL) containing a small amount of 1,3,5-trimethoxybenzene and recorded the ^{1}H NMR spectrum (Figure S14). We then recorded another ^{1}H NMR spectrum of the mixture after 2h at 50 °C (Figure S15) and examined changes in the integration of the aromatic TMB resonance (6.09 ppm) relative to the total imine resonances of **2a** and **2b**. The experiment confirmed that no significant changes occurred (total integral values of 2.45 (imines) vs 3.00 (TMB) before heating, compared to 2.42 vs 3.00 after heating), indicating no switching fatigue over this cycle.

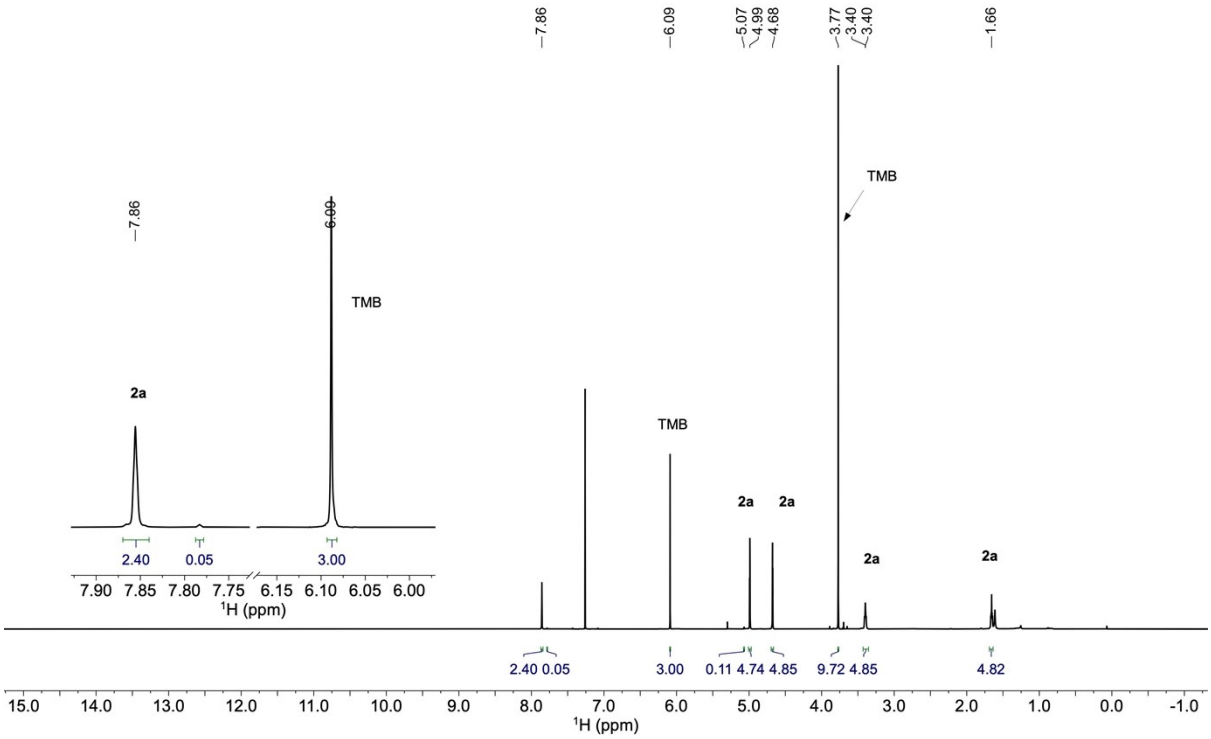

Figure S14. ^{1}H NMR spectrum of the mixture of **2a** and **2b** with internal standard of 1,3,5-trimethoxybenzene (TMB) before heating.

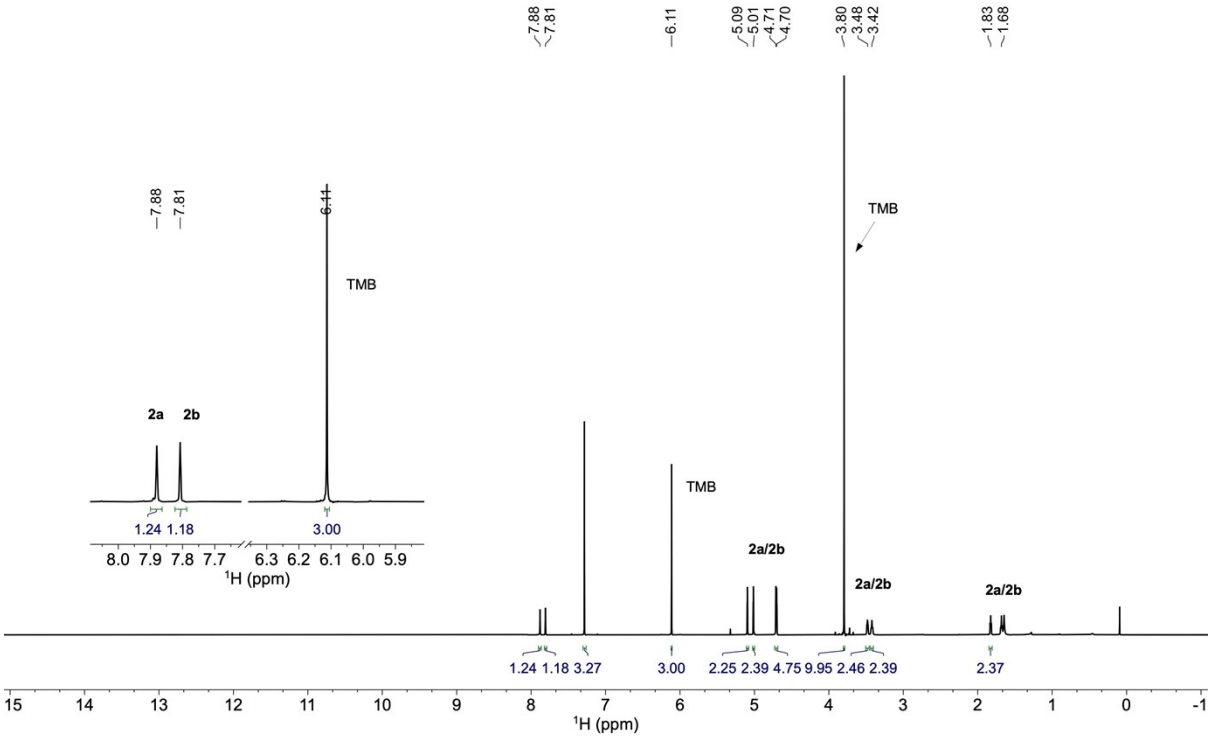

Figure S15. ^{1}H NMR spectrum of the mixture of **2a** and **2b** with internal standard of 1,3,5-trimethoxybenzene before heating, after heating for 2h to 50 °C.

1.4. of the Ruthenocenophane 2b as Diiminium-Cation

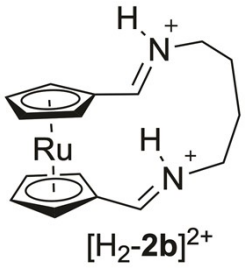

$[H_2$-**2b**$]^{2+}$

$[H_2$-**2b**$]^{2+}$: A 250 mL Schlenk flask equipped with a magnetic stirring bar and a reflux condenser was charged with macrocycle **2a** (50 mg, 0.07 mmol) and chloroform (50 mL). The slightly yellowish solution was refluxed for one hour. No colour changes were observed at this stage. The mixture was cooled to 0°C using an ice bath, and an excess of hydrochloric acid in ether (~ 1.0 M; 0.6 mL, 0.6 mmol) was added dropwise. Upon addition, the solution turned deep orange. Some precipitate formed during the reaction. The cooling bath was removed, the solution was allowed to warm to room temperature, and stirring was continued for another hour, after which most of the precipitate dissolved. The solution was taken up with a syringe and filtered through a syringe filter. The solvent was removed under reduced pressure, and the mixture was dried under a high vacuum (0.010 mbar), affording an orange crystalline solid (55 mg, 0.07 mmol, 99%). Single crystals of $[H_2$-**2b**$]^{2+}$ were obtained by slow

liquid diffusion of pentane into a solution in dichloromethane. This yielded two types of crystals, needles and platelets, [H_2-**2b**]Cl_2·2H_2O in its two modifications, which were selected using a microscope.

[H_2-**2b**]Cl_2·(H_5O_2)Cl: The dication [H_2-**2b**]$^{2+}$, co-crystallised with a Zundel cation and three chloride anions, was obtained similarly, on a smaller scale. A Schlenk tube, equipped with a magnetic stirring bar, was charged with macrocycle **2a** (5 mg, 0.007 mmol) and chloroform-*d* (5 mL). The mixture was stirred at 60 °C for 1 h and cooled to 0 °C. An excess of hydrochloric acid in ether (~ 1.0 M, 0.059 mmol, 0.06 mL) was added dropwise with a syringe. The product was filtered through a syringe filter and subsequently crystallised in an NMR tube by careful layering of the $CDCl_3$ solution with pentane and capping the tube under Ar. Standing overnight at room temperature produced single crystals suitable for X-ray diffraction. On air, the sensitive crystals became brittle and decomposed.

^{1}H NMR (400 MHz, $CDCl_3$) δ 13.47 (s, 2H, CHN*H*), 8.45 (d, *J* = 14.8 Hz, 2H, C*H*NH), 7.00 (m, 2H, Cp-*H*), 5.30 (m, 2H, Cp-*H*), 5.28 (m, 2H, Cp-*H*), 5.12 (m, 2H, Cp-*H*), 4.60 (m, 2H, butyl-*H*), 4.10 (m, 2H, butyl-*H*), 2.89 (m, 2H, butyl-*H*), 2.08 (m, 2H, butyl-*H*). MS(ESI+): 341 [M - H]$^+$ (100%).

1.5. Palladium-NHC Coordination to the Imines

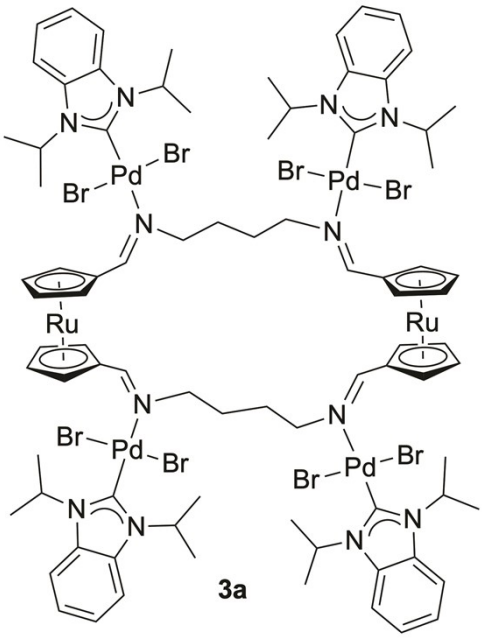

3a: A Schlenk tube, equipped with a magnetic stirring bar, was charged with **2a** (20 mg, 0.03 mmol) and acetonitrile (10 mL). The mixture was stirred at room temperature, producing a partial solution. Another Schlenk flask equipped with a magnetic stirring bar was charged with **[PdBr$_2$(^{i}Pr$_2$-bimy)]$_2$** (^{i}Pr$_2$-bimy = 1,3-diisopropylbenzimidazolin-2-ylidene) (55 mg, 0.06 mmol) and acetonitrile (10 mL). The mixture was stirred for 15 min at room temperature, upon which all solids dissolved, producing a clear yellow solution, which indicated the cleavage of the dimer **[PdBr$_2$(^{i}Pr$_2$-bimy)]2** to the monomer **[PdBr$_2$(MeCN)(^{i}Pr$_2$-bimy)]**. The acetonitrile mixture containing **2a** was taken up in a syringe and added dropwise, while stirring at room temperature, to the monomer solution **[PdBr2(MeCN)(^{i}Pr2-bimy)]**. After a few minutes of stirring, a light yellow precipitate began to form. Stirring was continued for two hours, after which the temperature was raised to 55°C and stirring was continued for another 2.5 h. The solution was allowed to cool down to room temperature, yielding a light yellow precipitate. The precipitate was collected using a glass frit, washed with acetonitrile (3 x 2 mL), and finally dried under vacuum. This afforded a light yellow crystalline material (42 mg, 0.02 mmol, 56 %). The compound is only sparingly soluble in a few common organic solvents (MeCN, dichloromethane, chloroform, or DMSO) and hardly soluble in others. We grew single crystals of **3a** from a dilute MeCN solution by slow solvent evaporation at room temperature. ^{1}H NMR (400 MHz, $CDCl_3$): δ 8.20 (s, 4H,

C*H*N), 7.57-7.54 (m, 8H, BzIm-*H*), 7.19-7.17 (m, 8H, BzIm-*H*), 6.42 (m, 4H, C*H*$(CH_3)_2$), 6.32 (m, 4H, C*H*$(CH_3)_2$), 6.09 (m, 8H, Cp-*H*), 4.95 (m, 8H, Cp-*H*), 3.89 (m, 8H, butyl-*H*), 2.38 (m, 8H, butyl-*H*), 1.78-1.77 (m, 48H, CH(C*H*$_3)_2$). ^{13}C NMR (151 MHz, $CDCl_3$) δ 166.7 (*C*HN), 163.7 (carbene-*C*), 133.7, 133.5, 122.2, 112.9, 112.7, 84.2 (ispo-*C*), 75.3, 73.9, 63.7, 54.9 (*C*H$(CH_3)_2$), 54.3 (*C*H$(CH_3)_2$), 28.9, 20.9 (CH(*C*H$_3)_2$), 20.8 (CH(*C*H$_3)_2$). MS(ESI+): 2488 (35%) [M – Br + Na]$^+$, 2438 (15%), 2235 (20%) [M – 4Br]$^+$, 2095 (78%) , 2053 (25%), 2015 (100%), 1973 (16%), 1626 (34%). HRMS (ESI$^+$): Calcd for $C_{84}H_{108}Br_7N_{12}[^{106}Pd]_4[^{102}Ru]_2$: 2464.7349; found: 2464.7356. Elemental analysis: Calcd for $C_{84}H_{108}Br_8N_{12}Pd_4Ru$: C, 39.5; H, 4.3; N, 6.6; found: C, 39.05; H, 4.1; N, 6.7.

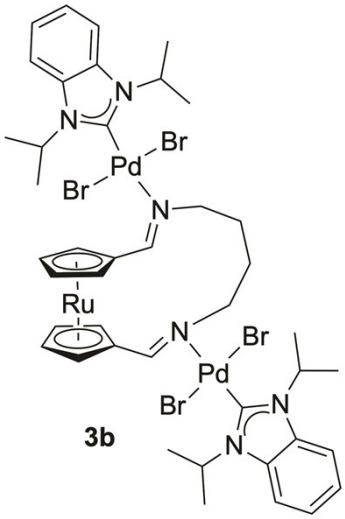

3b

The MeCN solutions from the filtration and washing of **3a** were combined and slowly evaporated at room temperature as well. This yielded crystals of ruthenocenophane **3b**, suitable for X-ray diffraction. The ^{1}H and ^{13}C NMR spectra of the solid indicated the presence of significant impurities, which included uncoordinated Pd-NHC species. We have not attempted further purification of it and characterised the title compound only by single crystal X-ray diffraction and mass spectrometry. MS (ESI$^+$): 1060 (100%) [M – 3Br + Na]$^+$. HRMS (ESI$^+$): Calcd for $C_{42}H_{54}Br_3N_6[^{106}Pd]_2[^{102}Ru]$: 1192.9080; found: 1192.9079.

1.6. Syntheses of 1,1'-Bis(*N*-isopropylmethaneimine)-ruthenocene

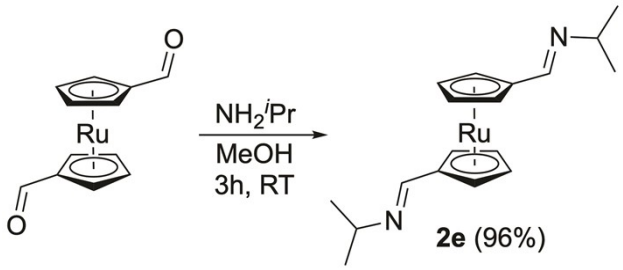

Scheme S2. Synthesis of 1,1'-Bis(*N*-isopropylmethaneimine)-ruthenocene (**2e**).

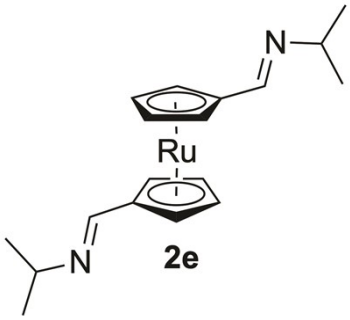

1,1'-Bis(*N*-isopropylmethaneimine)-ruthenocene (2e): On air, a round bottom flask equipped with a magnetic stirring bar was charged with **1** (100 mg, 0.35 mmol). Methanol (10 mL) was added, and the mixture was stirred at room temperature, producing a partial solution. An excess (5 equiv.) of the isopropylamine was added, and the mixture was stirred for three hours at room temperature. All remaining solids dissolved within several minutes, and the solution turned pale yellow. Subsequently, the solvent was removed using a rotary evaporator, and the product was dried under high vacuum. The crude solid was taken up in a few mL of pentane and filtered through a syringe filter into another round bottom flask. The solvent was again removed using a rotary evaporator, and the product was finally dried under high vacuum, giving a light yellow crystalline material (124 mg, 0.34 mmol, 96%). ^{1}H NMR (500 MHz, $CDCl_3$) δ 7.88 (s, 2H, C*H*N), 4.95 (pst, *J* = 1.8 Hz, 4H, Cp-*H*), 4.63 (d, *J* = 1.8 Hz, 4H, Cp-*H*), 3.27 (hept, *J* = 6.2 Hz, 2H, C*H*(CH_3)$_2$), 1.13 (d, *J* = 6.4 Hz, 12H, CH(C*H*$_3$)$_2$). ^{13}C NMR (126 MHz, $CDCl_3$) δ 156.1 (*C*HN), 86.4 (*ipso*-C), 73.0 (Cp-*C*), 71.5 (Cp-*C*), 61.7 (*C*H(CH_3)$_2$), 24.1 (CH(*C*H$_3$)$_2$) ppm. MS(ESI+): 371 [*M* + H]$^+$ (100%). HRMS (ESI+): Calcd for

$C_{18}H_{25}N_2[^{102}Ru]$: 371.1061; found: 371.1059. Elemental analysis: Calcd for $C_{18}H_{24}N_2Ru$: C, 58.5; H, 6.6; N, 7.6; found: C, 58.2; H, 6.4; N, 7.7.

2. Switching Experiments

Macrocycle **2a** (3 mg, 4.4 µmol) was weighed into a vial and dissolved in chloroform-*d* (1 mL). The solution was taken up in a syringe, filtered through a syringe filter into an argon-flushed NMR tube (0.5 mL volume), which was capped under a stream of argon. The sample was loaded into the NMR spectrometer, locked, shimmed, and a first spectrum was recorded at room temperature. Subsequently, the probe head temperature was raised to 50 °C while the sample was in the magnet. Once 50 °C had been reached, ^{1}H NMR spectra were recorded. Each spectrum was recorded with 8 scans, followed by a fixed 2 min interval before the next spectrum was recorded.

For the first run, in total 41 spectra were recorded: the first at room temperature, and the remaining at 50°C. Once the run was completed, the sample was removed from the spectrometer and stored in a fridge at -25 °C for several days. After this, the sample was allowed to warm up to room temperature, an NMR spectrum was recorded at room temperature, and the sample was heated up again. For the subsequent runs, 15 NMR spectra were recorded. Two sets of experiments were conducted, with chloroform-*d* distilled from CaH_2 (Series A). treated with K_2CO_3 (Series B). Determination of the relative content of **2a** and **2b** to each other, the imine resonances of **2a** and **2b** were quantified by integration with respect to each other.

Figures S16-19 show the stacked plots of ^{1}H NMR spectra of Series A and the corresponding relative ratios are shown in Figure 1c (main manuscript). The relative ratios of Series B are shown in Figure S19 and Figures S20-26 show the corresponding stacked plot of ^{1}H NMR spectra of Series B.

Series A ($CDCl_3$ dried from CaH_2)

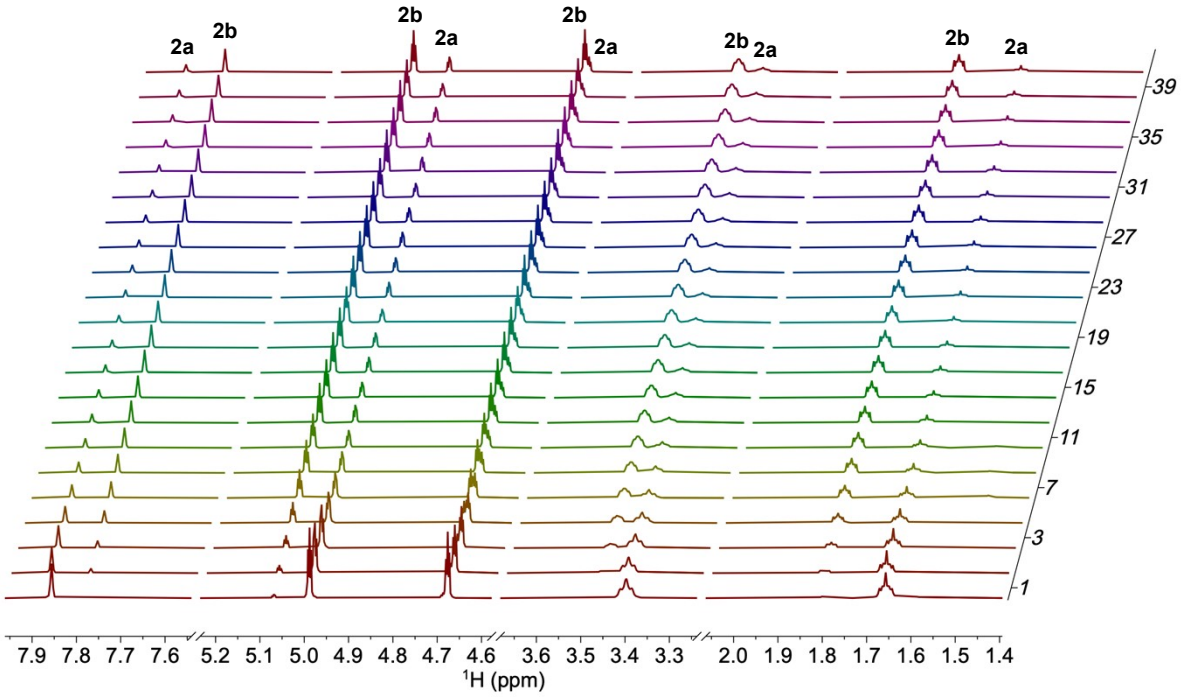

Figure S16. Run 1 of the thermally induced switching from **2a** to **2b**, monitored by VT NMR spectroscopy. The first spectrum was recorded at room temperature, and all subsequent spectra were recorded at 50 °C. The spectra were recorded in intervals of two minutes. For clarity, from spectrum three onwards, only every second spectrum is shown.

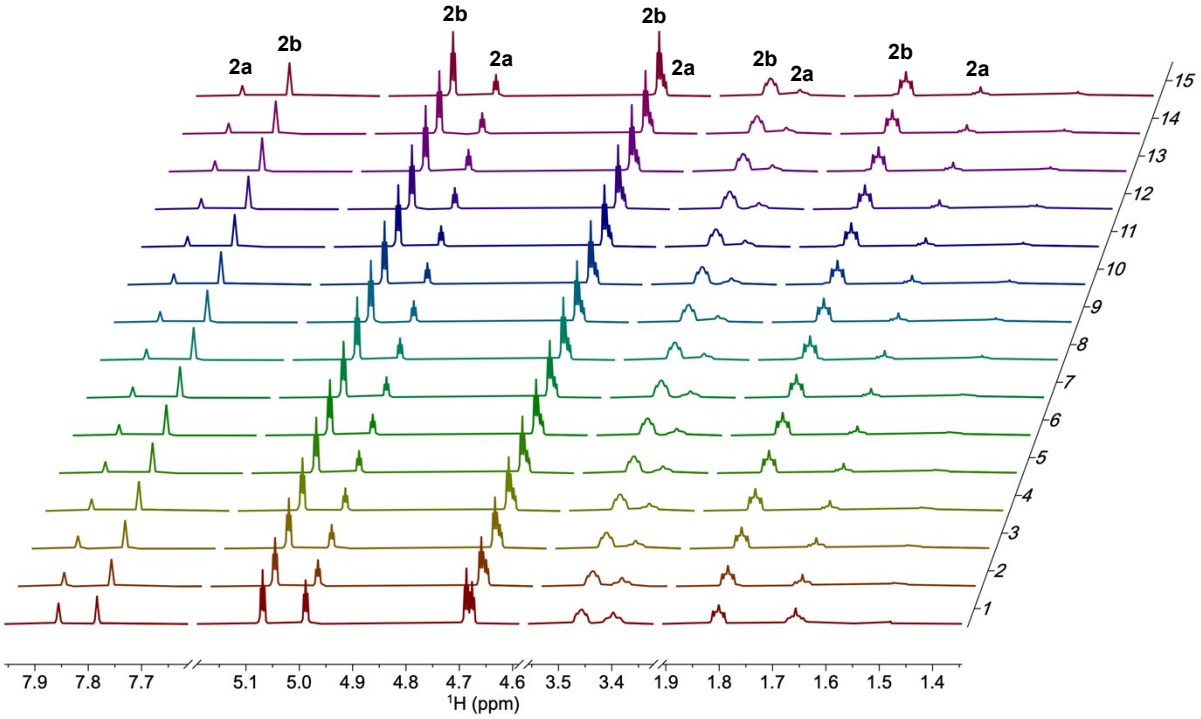

Figure S17. Run 2 of the thermally induced switching from **2a** to **2b**, monitored by VT NMR spectroscopy. The first spectrum was recorded after storing the sample

from run 1 for three days at -25 °C. The spectra were recorded in intervals of two minutes. For clarity, from spectrum 3 onwards, only every third spectrum is shown.

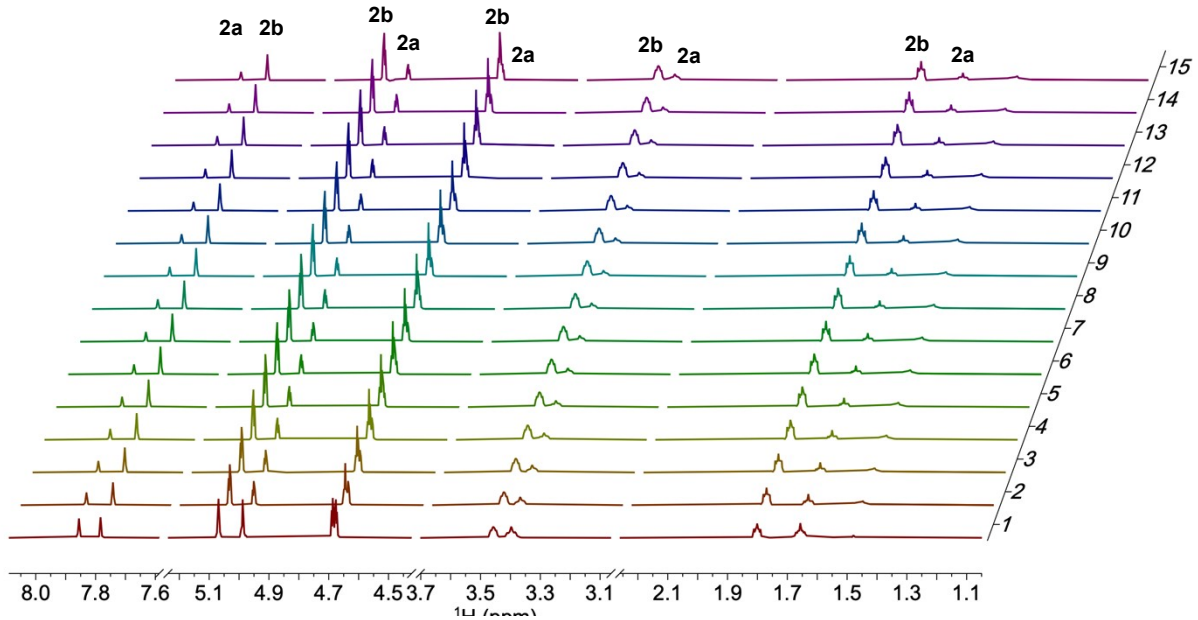

Figure S18. Run 3 of the thermally induced switching from **2a** to **2b**, monitored by VT NMR spectroscopy. The first spectrum was recorded after storing the sample from run 2 for three days at -25 °C. The spectra were recorded in intervals of two minutes. For clarity, only every third spectrum is shown.

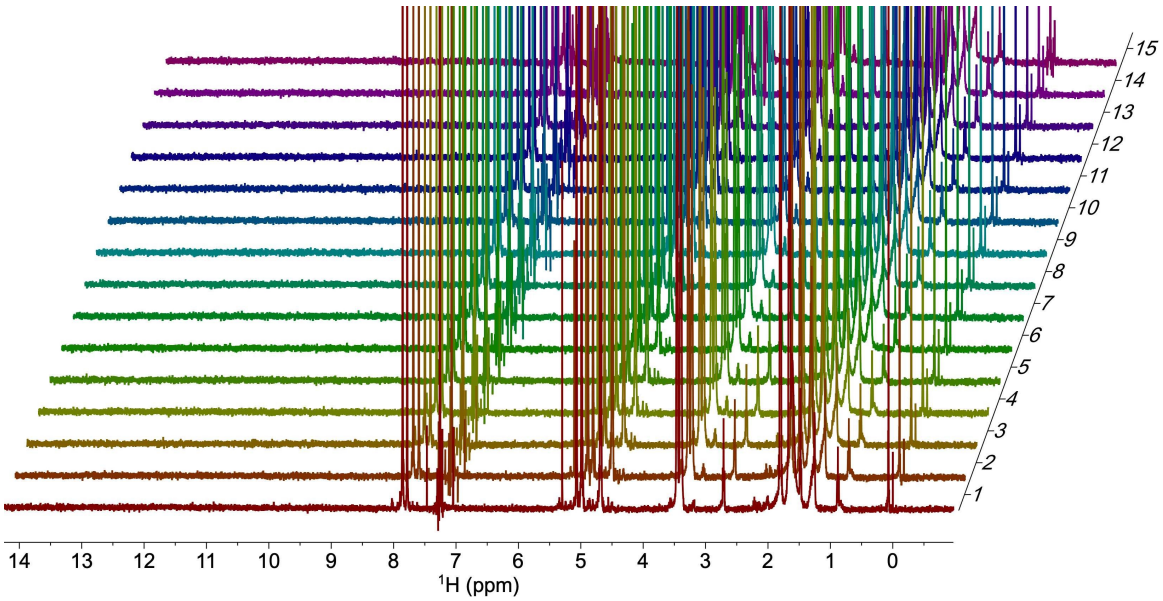

Figure S19. Run 3 of the thermally induced switching from **2a** to **2b**, monitored by VT NMR spectroscopy; larger magnification. No aldehyde signals are evident after the three subsequent cycles.

Series B ($CDCl_3$ treated with K_2CO_3)

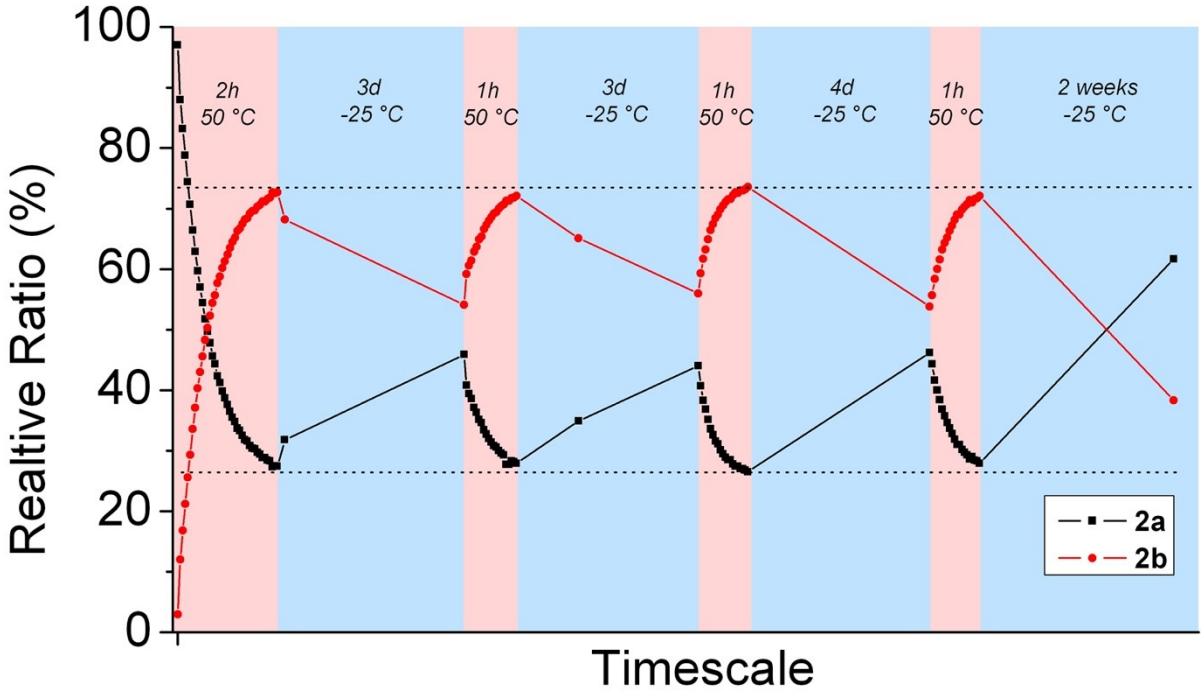

Figure S20. Thermally induced switching between **2a** and **2b**, in K_2CO_3 treated $CDCl_3$. The timescale is not to scale for the heating and cooling cycles.

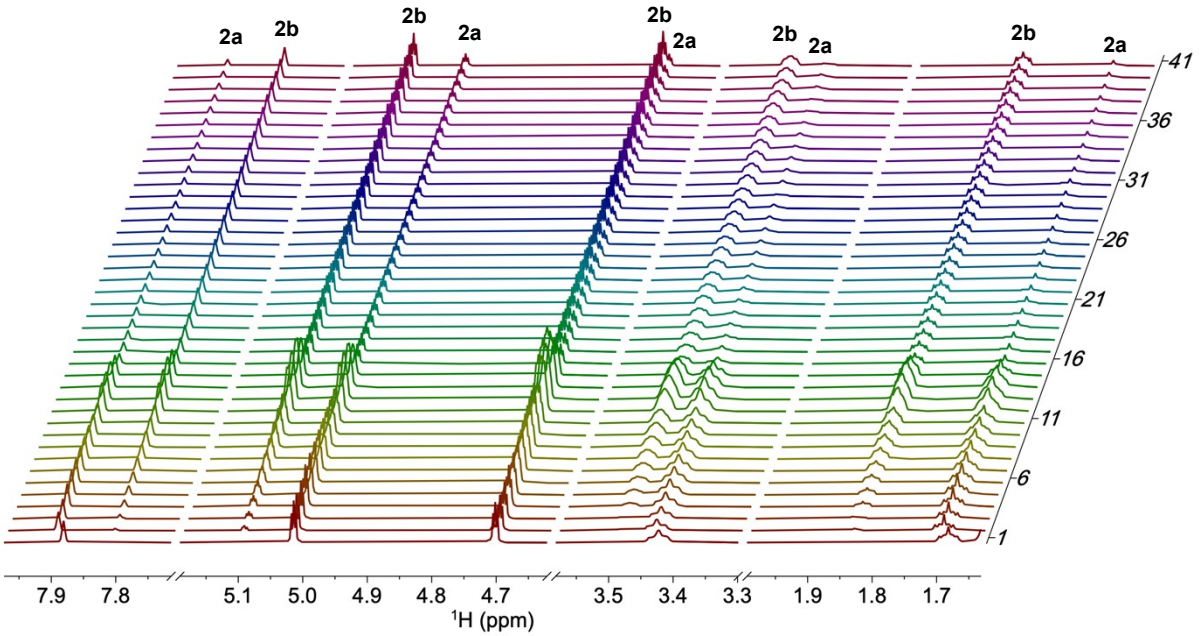

Figure S21. Run 1 of the thermally induced switching from **2a** to **2b**, monitored by VT NMR spectroscopy. The spectra were recorded in intervals of two minutes. Initially, the shim was affected by the raised temperature, which led to a broadening of signals up to spectrum 16, after which auto-shimming was turned on, which was used for all subsequent measurements. This improved the signal quality significantly. We furthermore note that one spectrum of the series was discarded due to an instrument error (not shown).

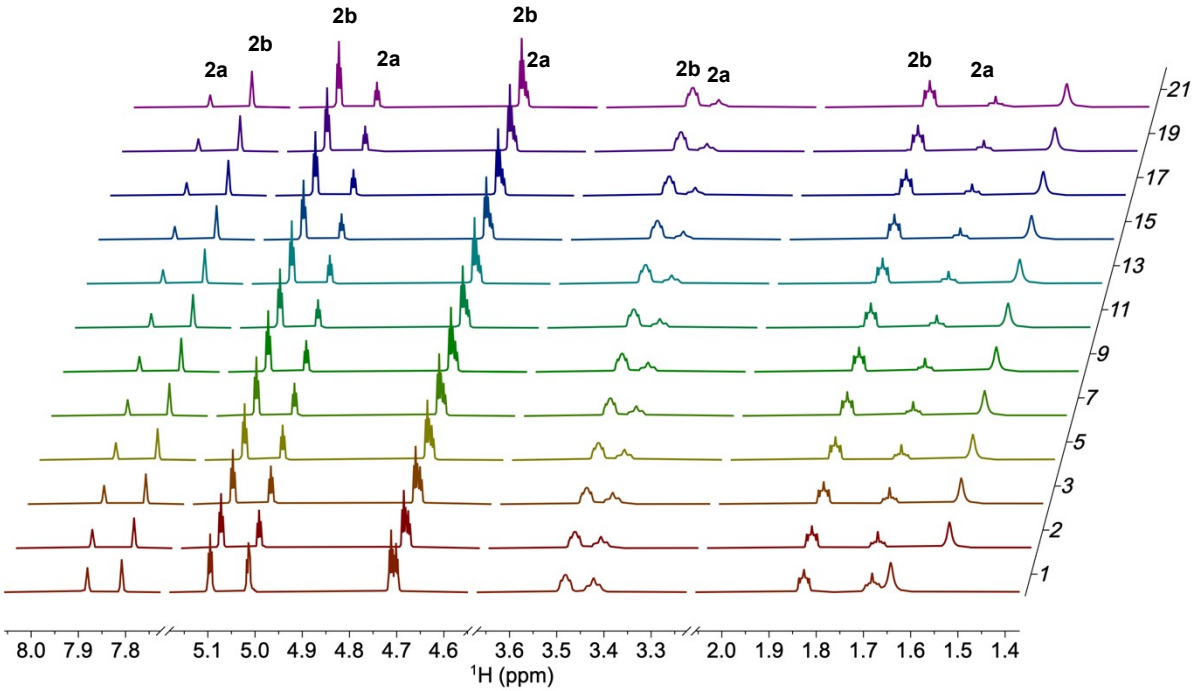

Figure S22. Run 2 of the thermally induced switching from **2a** to **2b**, monitored by VT NMR spectroscopy. The first spectrum was recorded at room temperature after storing the sample after run 1 for three days at -25 °C, and all subsequent spectra were recorded at 50 °C. The spectra were recorded in intervals of two minutes. For clarity, from spectrum three onwards, only every second spectrum is shown.

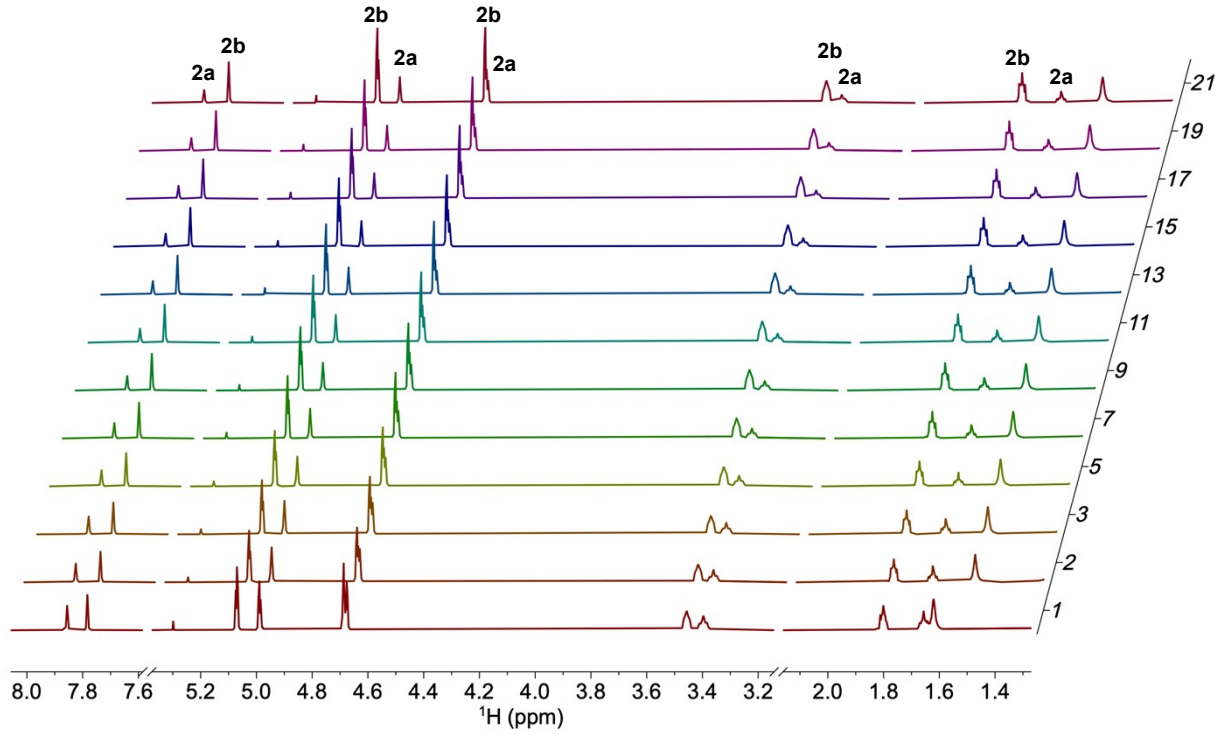

Figure S23. Run 3 of the thermally induced switching from **2a** to **2b**, monitored by VT NMR spectroscopy. The first spectrum was recorded at room temperature after storing the sample after run 2 for three days at -25 °C, and all subsequent spectra were recorded at 50 °C. The spectra were recorded in intervals of two minutes. For clarity, from spectrum three onwards, only every second spectrum is shown.

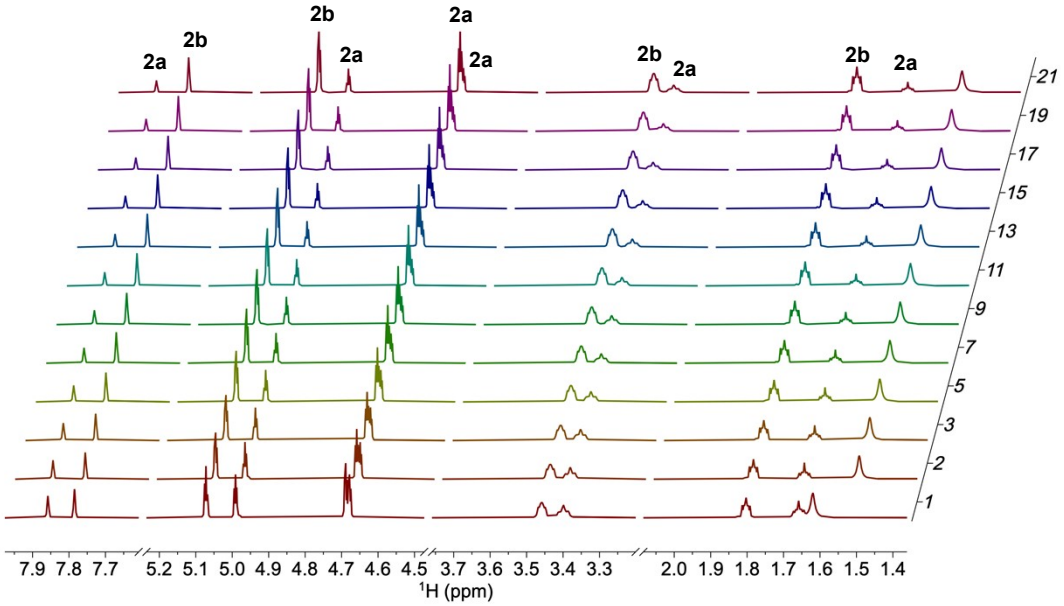

Figure S24. Run 4 of the thermally induced switching from **2a** to **2b**, monitored by VT NMR spectroscopy. The first spectrum was recorded at room temperature after storing the sample after run 3 for four days at -25 °C, and all subsequent spectra were recorded at 50 °C. The spectra were recorded in intervals of two minutes. For clarity, from spectrum three onwards, only every second spectrum is shown.

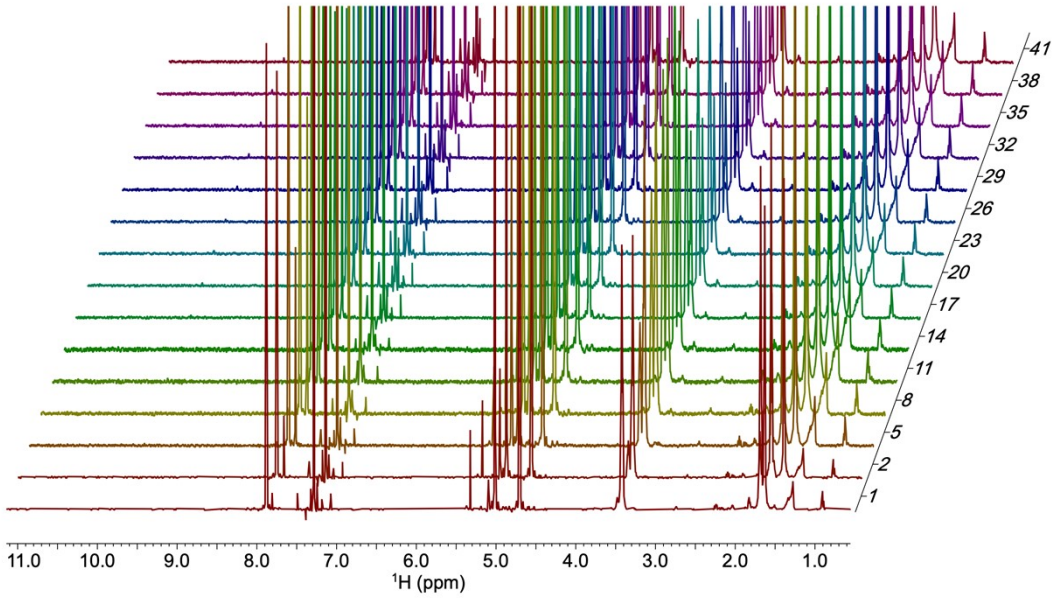

Figure S25. Run 1 of the thermally induced switching from **2a** to **2b**, monitored by VT NMR spectroscopy; larger magnification. The low-intensity signal at approximately 9.7 ppm, from spectrum 20 onwards, is likely corresponding to aldehyde proton signals in trace amounts.

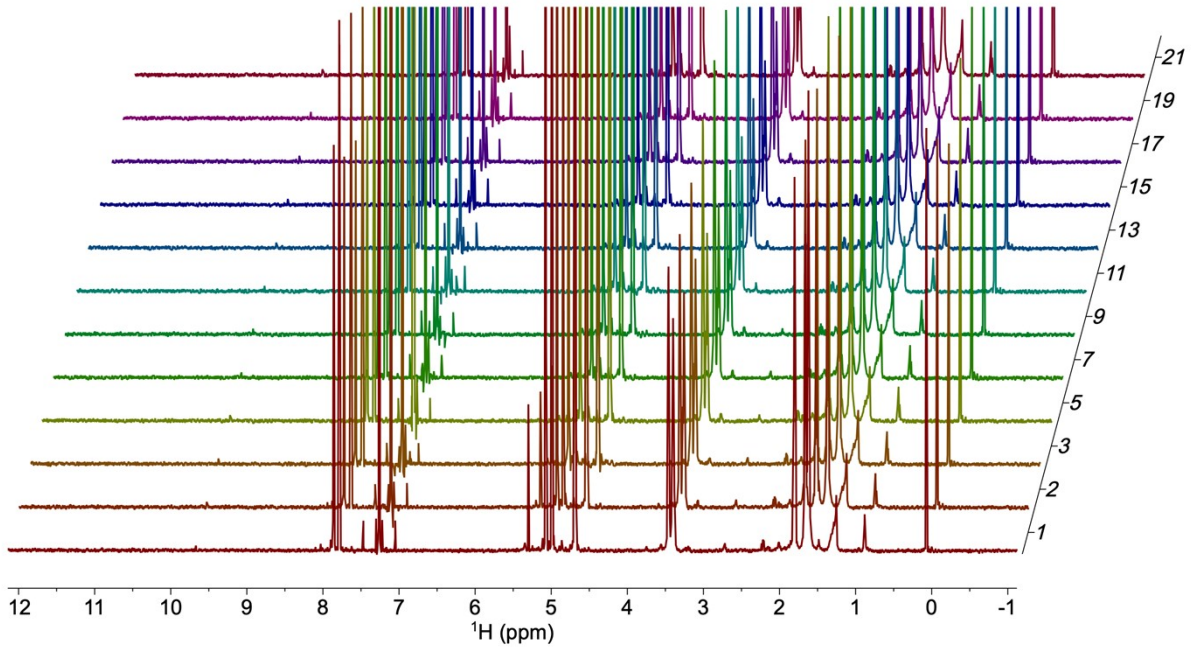

Figure S26. Run 4 of the thermally induced switching from **2a** to **2b**, monitored by VT NMR spectroscopy; larger magnification. The low-intensity signal at approximately 9.7 ppm, from spectrum 20 onwards, is likely corresponding to aldehyde proton signals in trace amounts.

Control Experiments

Reaction with n-Propylamine

A Schlenk tube equipped with a magnetic stirring bar was charged with macrocycle **2a** (4 mg, 0.006 mmol), *n*-propylamine (3.5 mg, 0.060 mmol), and chloroform-*d* (4 mL). The mixture was heated to 60°C while stirring for one hour. An aliquot was taken and analysed by ^{1}H NMR spectroscopy. Selected regions of the ^{1}H NMR spectrum are shown in Figure S27. The remainder was concentrated to dryness and dried under high vacuum. The sample was analysed again by ^{1}H NMR spectroscopy in chloroform-*d* (Figure S28) and by mass spectrometry. The ^{1}H NMR spectrum before vacuum drying contains an excess of *n*-propylamine. It confirms the presence of different imine protons with resonances at 7.86 and 7.78 ppm, and several signals for the Cp-protons from 5.07 - 4.67 ppm. All these Cp resonances exhibit, as expected, chemical shifts similar to those of **2a**/**2b**, as the chemical environments of the Cp-H in **2c**/**2d** are very similar to those of **2a**. In contrast, distinct differences are visible in the aliphatic region, with different coupling patterns observed. The signals at 3.46 ppm are assigned to **2b,** while the weak signal of 3.37 ppm is assigned to **2a**. The multiplet at 3.33 ppm is assigned to the scrambling products arising from the CH_2-unit adjacent to the formed *n*-propylimines. Concentration and drying again altered the composition of the mixture as the system equilibrated after solvent evaporation. The signal at 3.37 ppm increased in intensity relative to that at 3.47 ppm, confirming that **2b** had been back-converted to **2a**. The triplet at 0.91 ppm indicates the presence of *n*-propyl groups in the components of the sample. Mass spectrometric analysis (Figure S29) confirmed the masses of the following compounds: **2a** (m/z = 341), the ruthenocenophane **2b** (m/z = 680), *n*-propyl derivatives **2c** (m/z = 317) and **2d** (m/z = 709).

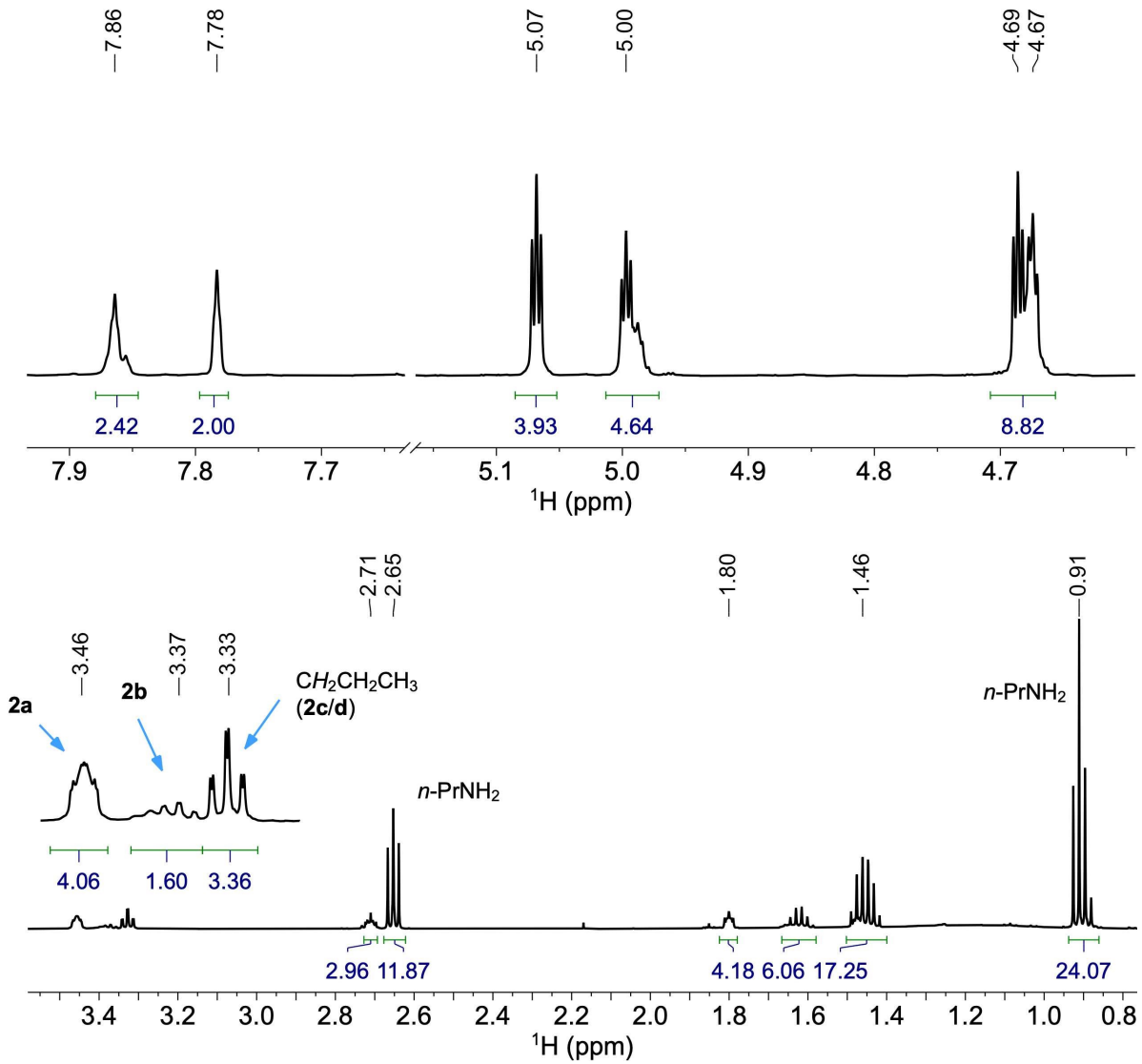

Figure S27. Selected regions of the ^{1}H NMR spectrum of the mixture obtained from heating **2a** for one hour at 60 °C with an excess of *n*-propylamine. The excess of *n*-propylamine is visible in the aliphatic region and indicated.

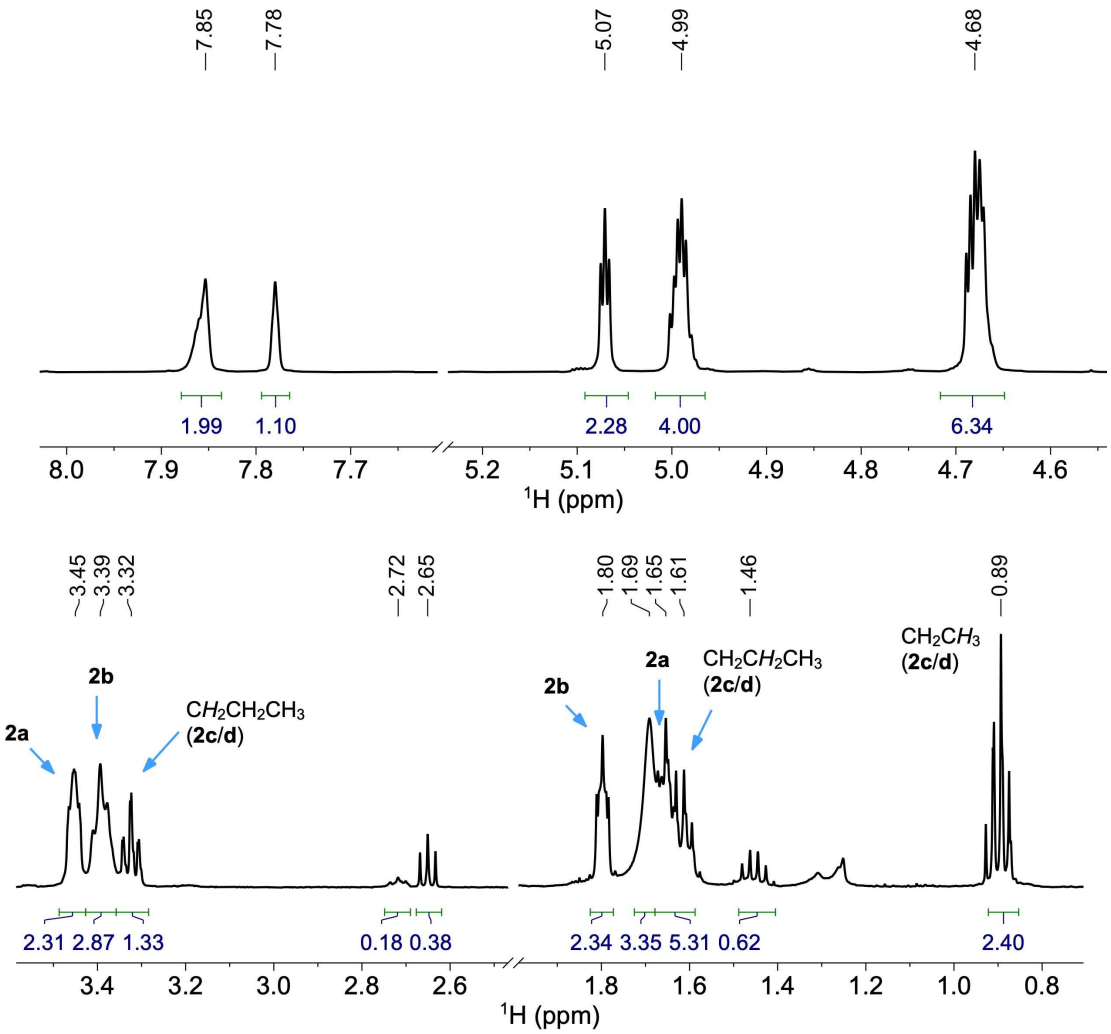

Figure S28. Selected regions of the ^{1}H NMR spectrum of the mixture obtained from heating of **2a** for one hour at 60 °C with an excess of *n*-propylamine, after drying under high vacuum.

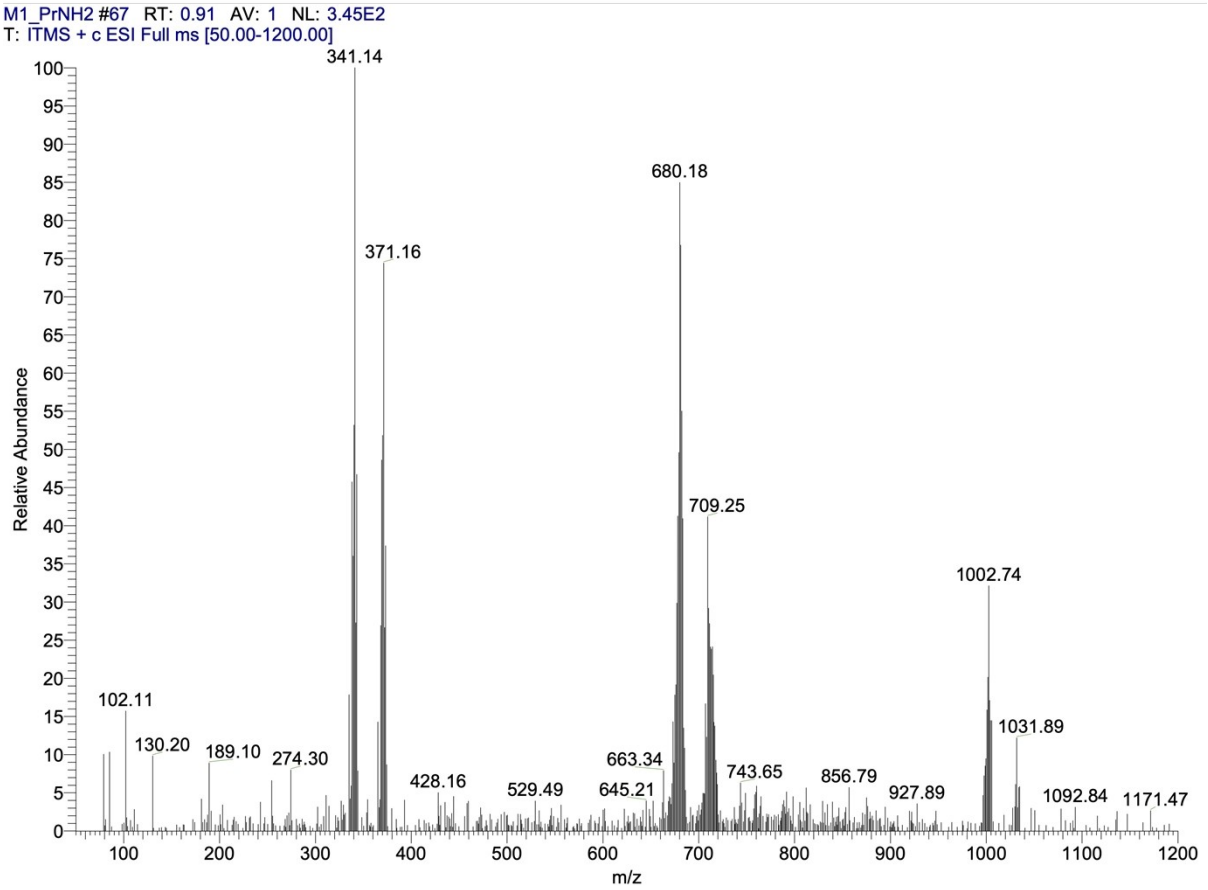

Figure S29. ESI$^+$ mass spectrum of the mixture obtained from heating of **2a** for 1h at 60 °C with an excess of *n*-propylamine. The molecular peaks for the different imines are indicated (m/z = 341 (**2b**), 317 (**2c**), 680 (**2a**), 709 (**2d**)). The peak at m/z 1003 was not assigned.

Attempted Reaction with 1,1'-Bis(N-isopropylimine)-ruthenocene (**2d**)

A Schlenk tube equipped with magnetic stirring bar was charged with macrocycle **2a** (2.0 mg, 0.003 mmol), an excess of **2d** (2.2 mg, 0.06 mmol), and chloroform-*d* (4 mL). The mixture was heated to 60°C while stirring for one hour, and was subsequently analysed by ^{1}H NMR spectroscopy. No imine scrambling occurred, and the **2a**/**b** ratio was 86/14, indicating that no significant amount of **2b** was generated during heating, as the reaction isomerisation was inhibited. Selected regions of the ^{1}H NMR spectrum are shown in Figure S30.

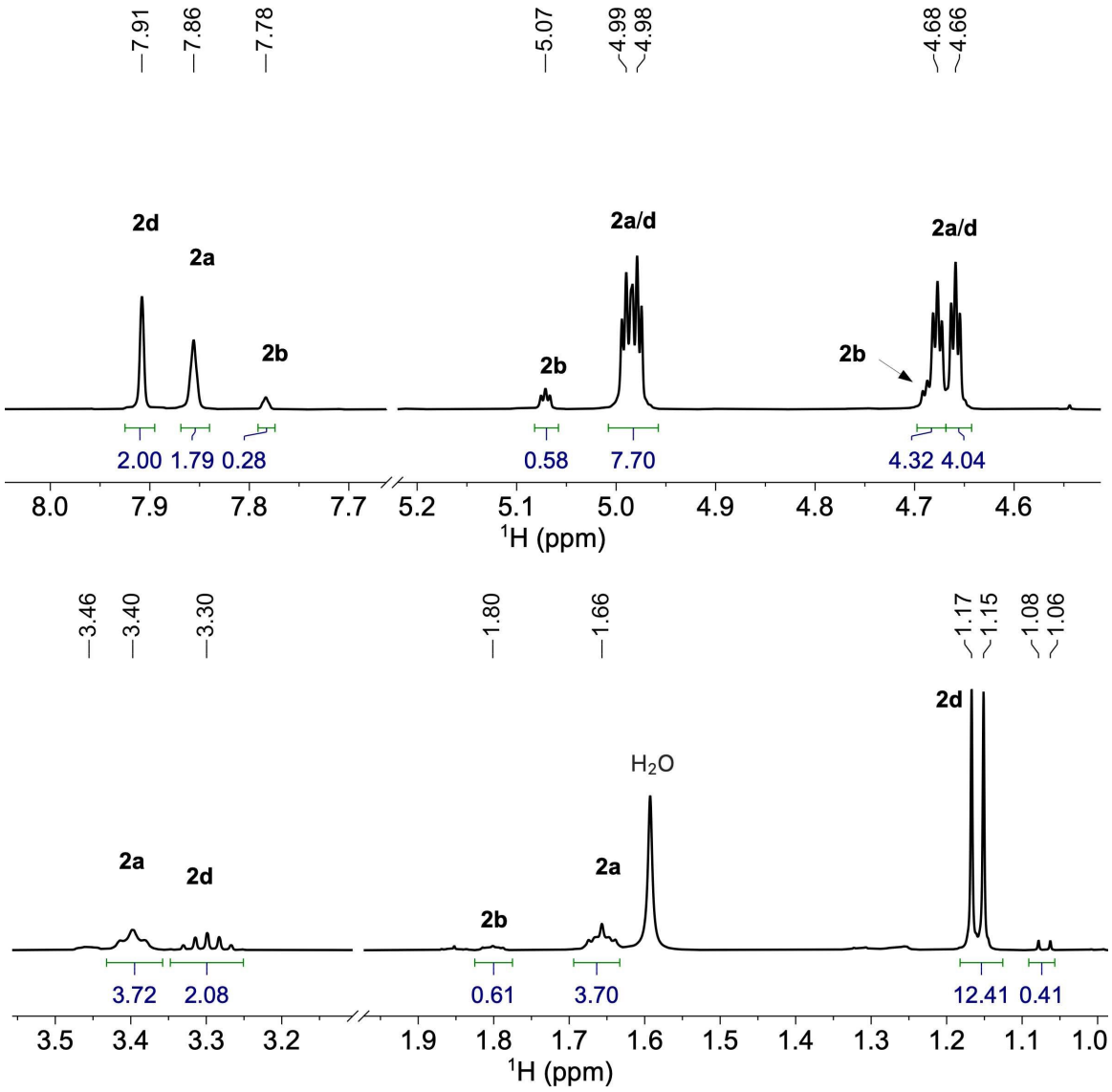

Figure S30. Selected regions of the ^{1}H NMR spectrum of a mixture of **2a** and **2d**, after heating for one hour at 60 °C. Only a minor amount of **2b** is present.

3. Details from the Single Crystal X-ray Diffraction Experiments

Single crystal X-ray diffraction was carried out on a Bruker D8 Venture single crystal X-ray diffractometer. Suitable crystals were selected, affixed to a capillary loop using an optical microscope, mounted on the diffractometer, and measured. The experimental data are summarised in Tables S1 and S2. **Table S1.** Details of the X-ray structure determinations for the different crystals of **2a** and [H_2-**2b**]Cl_2·(H_5O_2)Cl.

Compound	**2a**·CH_2Cl_2	**2a**	**2a**·H_2O	[H_2-**2b**]Cl_2·(H_5O_2)Cl
CCDC-Number	2520939	2520940	2520941	2520942
Empirical formula	$C_{33}H_{38}Cl_2N_4Ru_2$	$C_{32}H_{36}N_4Ru_2$	$C_{32}H_{40}N_4O_2Ru_2$	$C_{16}H_{25}Cl_3N_2O_2Ru$
Formula weight	763.71	678.79	714.82	484.8
Temperature / K	100.00	100(2)	100.00	100(2)
Wavelength / Å	0.71073	0.71073	0.71073	0.71073
Crystal system	Orthorhombic	Triclinic	Monoclinic	Monoclinic
Space group	Iba2	P-1	$P2_1/c$	$P2_1/n$
a / Å	25.0012(14)	5.8912(6)	17.9581(9)	7.4956(4)
b / Å	25.0261(15)	7.8003(8)	8.9738(4)	26.0490(15)
c / Å	10.1797(7)	14.8669(15)	9.2136(4)	10.2702(5)
α / °	90	97.445(4)	90	90
β / °	90	94.279(5)	103.431(2)	101.442(2)
γ / °	90	94.109(5)	90	90
Volume / Å^3	6369.3(7)	673.24(12)	1444.18(12)	1965.43(18)
Z	8	1	2	4
Density (calculated) g/cm^3	1.593	1.674	1.644	1.638
Absorption coefficient / mm^{-1}	1.145	1.151	1.082	1.217
F(000)	3088	344	728	984
Crystal size / mm^3	0.242 x 0.119 x 0.082	0.201 x 0.138 x 0.046	0.112 x 0.073 x 0.06	0.132 x 0.122 x 0.078
Theta range for data collection	2.160 to 29.585°	2.642 to 29.762°	2.332 to 30.523°	2.557 to 29.608°.
Index ranges	-33<=h<=34 -34<=k<=34 -14<=l<=14	-8<=h<=8, -10<=k<=10, 0<=l<=20	-25<=h<=25, -12<=k<=12, -13<=l<=11	-10<=h<=10, 36<=k<=36, -14<=l<=11
Reflections collected	158084	5461	53002	48200
Independent reflections	8936 [$R_{(int)}$ = 0.0996]	5461 [$R_{(int)}$ = n/a]	4413 [$R_{(int)}$ = 0.0530]	5515 [$R_{(int)}$ = 0.0504]
Completeness to theta = 25.242°	99.80%	98.20%	100.00%	99.90%
Absorption correction	Semi-empirical from equivalents	Semi-empirical from equivalents	Semi-empirical from equivalents	Semi-empirical from equivalents
Max. and min. transmission	0.7459 and 0.6787	0.745908 and 0.655361	0.7461 and 0.6964	0.7459 and 0.6843
Refinement method	Full-matrix least-squares on F^2	Full-matrix least-squares on F^2	Full-matrix least-squares on F^2	Full-matrix least-squares on F^2
Data / restraints / parameters	8936 / 1 / 371	5461 / 676 / 336	4413 / 1 / 187	5515 / 0 / 243
Goodness-of-fit on F^2	1.075	1.118	1.05	1.038
Final R indices [I>2σ(I)]	R_1 = 0.0252 wR_2 = 0.0573	R_1 = 0.0490 wR_2 = 0.0994	R_1 = 0.0211 wR_2 = 0.0507	R_1 = 0.0253 wR_2 = 0.0591
R indices (all data)	R_1 = 0.0256 wR_2 = 0.0576	R_1 = 0.0570 wR_2 = 0.1060	R_1 = 0.0246 wR_2 = 0.0532	R_1 = 0.0323 wR_2 = 0.0625
Largest diff. peak and hole / *e*Å^{-3}	1.165 and -0.311	1.009 and -0.760	0.521 and -0.410	0.617 and -0.351

Table S2. Details of the X-ray structure determinations for the two different modifications of [H_2-**2b**]Cl_2·$2H_2O$, **3a** and **3b**.

Compound	[H_2-**2b**]Cl_2·$2H_2O$	[H_2-**2b**]Cl_2·$2H_2O$	**3a**	**3b**
CCDC-Number	2520943	2520944	2520945	2520946
Empirical formula	$C_{16}H_{24}Cl_2N_2O_2Ru$	$C_{16}H_{20.50}Cl_2N_2O_{0.25}Ru$	$C_{86}H_{111}Br_8N_{13}Pd_4Ru_2$	$C_{46}H_{60}Br_4N_8Pd_2Ru$
Formula weight	448.34	416.81	2593.89	1358.53
Temperature / K	100.00 K	100.00 K	100.00 K	100.00 K
Wavelength / Å	0.71073 Å	0.71073 Å	1.54178 Å	0.71073 Å
Crystal system	Monoclinic	Monoclinic	Monoclinic	Monoclinic
Space group	$P2_1/n$	C2/c	$P2_1/n$	$P2_1/c$
a / Å	7.0835(5)	6.9208(3)	12.2104(5)	18.3955(8)
b / Å	16.3005(13)	17.5059(9)	17.8590(7)	15.8791(6)
c / Å	15.2698(9)	13.8124(7)	23.2698(8)	17.6057(7)
α / °	90	90	90	90
β / °	91.464(2)	97.074(2)	93.341(2)	97.568(2)
γ / °	90	90	90	90
Volume Å^3	1762.5(2)	1660.70(14)	5065.7(3)	5097.9(4)
Z	4	4	2	4
Density (calculated) g/cm^3	1.690	1.667	1.701	1.770
Absorption coefficient / mm^{-1}	1.203	1.262	12.012	4.165
F(000)	912	842	2540	2672
Crystal size / mm^3	0.102 x 0.039 x 0.034	0.174 x 0.099 x 0.061	0.088 x 0.073 x 0.029	0.148 x 0.134 x 0.07
Theta range for data collection	2.499 to 28.347°.	2.327 to 29.585°.	3.121 to 70.468°.	2.234 to 28.306°.
Index ranges	-9<=h<=9 -21<=k<=21 -20<=l<=17	-6<=h<=9 -24<=k<=24 -19<=l<=19	-14<=h<=14 -21<=k<=21 -28<=l<=28	-24<=h<=24 -21<=k<=20 -23<=l<=23
Reflections collected	62883	17533	87335	170309
Independent reflections	4410 [$R_{(int)}$ = 0.1164]	2342 [$R_{(int)}$ = 0.0474]	9656 [$R_{(int)}$ = 0.0771]	12666 [$R_{(int)}$ = 0.0787]
Completeness to theta = 25.242°	100.00%	99.90%	99.90%	99.90%
Absorption correction	Semi-empirical from equivalents	Semi-empirical from equivalents	Semi-empirical from equivalents	Semi-empirical from equivalents
Max. and min. transmission	0.7221 and 0.6750	0.7459 and 0.6831	0.7533 and 0.6118	0.7457 and 0.6742
Refinement method	Full-matrix least-squares on F^2	Full-matrix least-squares on F^2	Full-matrix least-squares on F^2	Full-matrix least-squares on F^2
Data / restraints / parameters	4410 / 2 / 226	2342 / 0 / 107	9656 / 42 / 560	12666 / 132 / 597
Goodness-of-fit on F^2	1.023	1.05	1.07	1.044
Final R indices [I>2σ(I)]	R_1 = 0.0380 wR_2 = 0.0856	R_1 = 0.0224 wR_2 = 0.0509	R_1 = 0.0471 wR_2 = 0.1354	R_1 = 0.0343 wR_2 = 0.0841
R indices (all data)	R_1 = 0.0530 wR_2 = 0.0949	R_1 = 0.0250 wR_2 = 0.0526	R_1 = 0.0564 wR_2 = 0.1426	R_1 = 0.0499 wR_2 = 0.0922
Largest diff. peak and hole / *e*Å^{-3}	2.477 and -0.630	0.497 and -0.290	1.474 and -1.124	3.035 and -0.811

Important bond lengths and angles of Zundel ion in [H_2-**2b**]Cl_2·(H_5O_2)Cl are reported in Table S3.

Table S3. Important bond lengths (Å) and angles (°) of the Zundel cation. The positions of the H-atoms were obtained from the diffraction map and refined.

Bonds	D–H [a]	H···A [b]	D–H···A [c]	Angle
O1–H1B···Cl2	0.89(3)	2.12(3)	3.004(2)	172(3)
O1–H1C···Cl1	0.92(3)	2.00(3)	2.016(2)	172(2)
O1–H1D–O2	1.14(4)	-	2.428(2)	175(3)
O1–H1D–O2	1.29(4)	-	2.428(2)	175(3)
O2–H2B···Cl3	0.96(3)	2.01(3)	2.943(2)	164(3)
O2–H2C···Cl2	0.84(3)	2.19(3)	3.028(2)	172(3)

[a] Covalent bond, [b] Hydrogen bond, [c] Distance between the terminal atoms of the three atoms.

One chloride is the bridge between two Zundel cations, forming two-dimensional chains in the crystal (Figure S31). The H-bonds to this bridging chloride ion are slightly larger (2.12(3) and 2.19(3) Å) compared to the two non-bridging chlorides (2.00(3) and 2.01(3) Å). These distances agree with a previous report of a chloride-stabilised Zundel cation.[6] The bonds between the bridging hydrogen H1D and O1 and O2 are 1.15(4) and 1.29(4) Å, respectively. This indicates that the H-atom is not exactly midway between the two oxygen atoms. Furthermore, the three atoms deviate from linearity with an angle of 175(3)°, in agreement with a reported nitranilic acid structure.[7] Packing in the crystal for the cationic ruthenocenophane [H_2-**2b**]Cl_2·(H_5O_2)Cl is illustrated in Figure S31. The packing of the two modifications of [H_2-**2b**]Cl_2·2H_2O is illustrated in Figure S32.

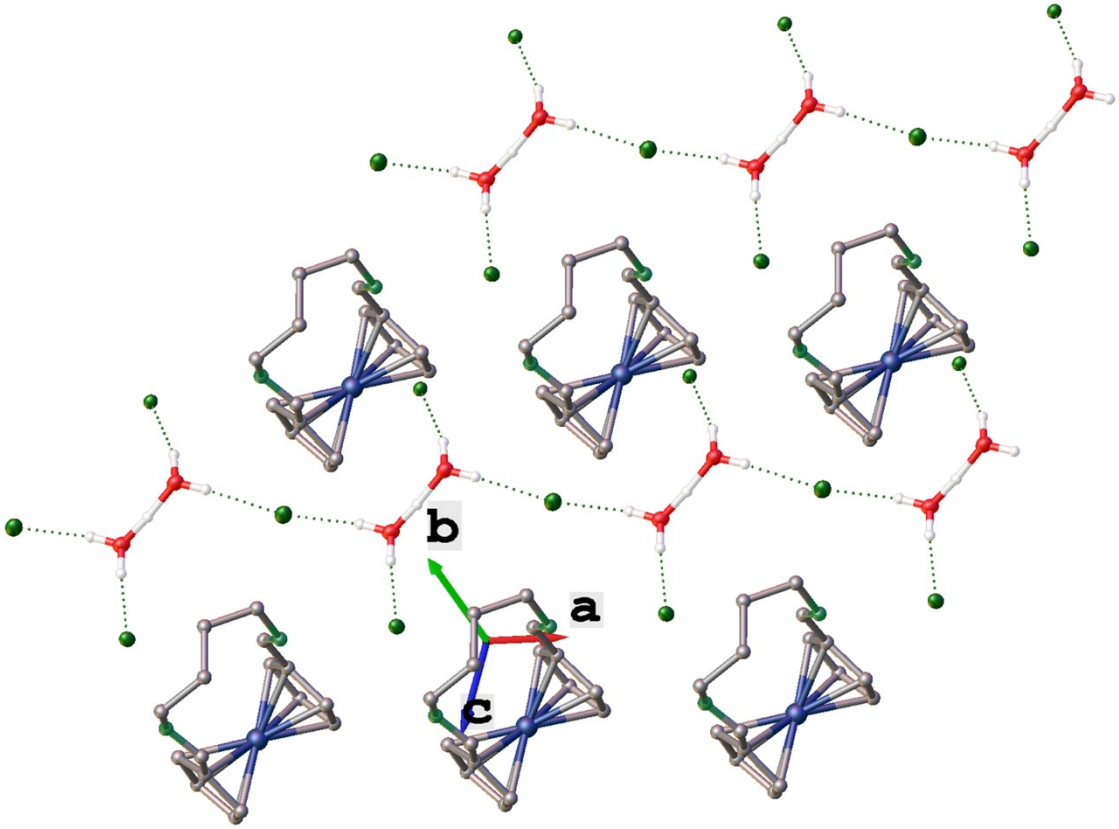

Figure S31. Packing of [H_2-**2b**]Cl_2·(H_5O_2)Cl in the crystal. The Zundel cation is stabilised through H-bonding with three chloride ions, forming infinite chains in the crystal.

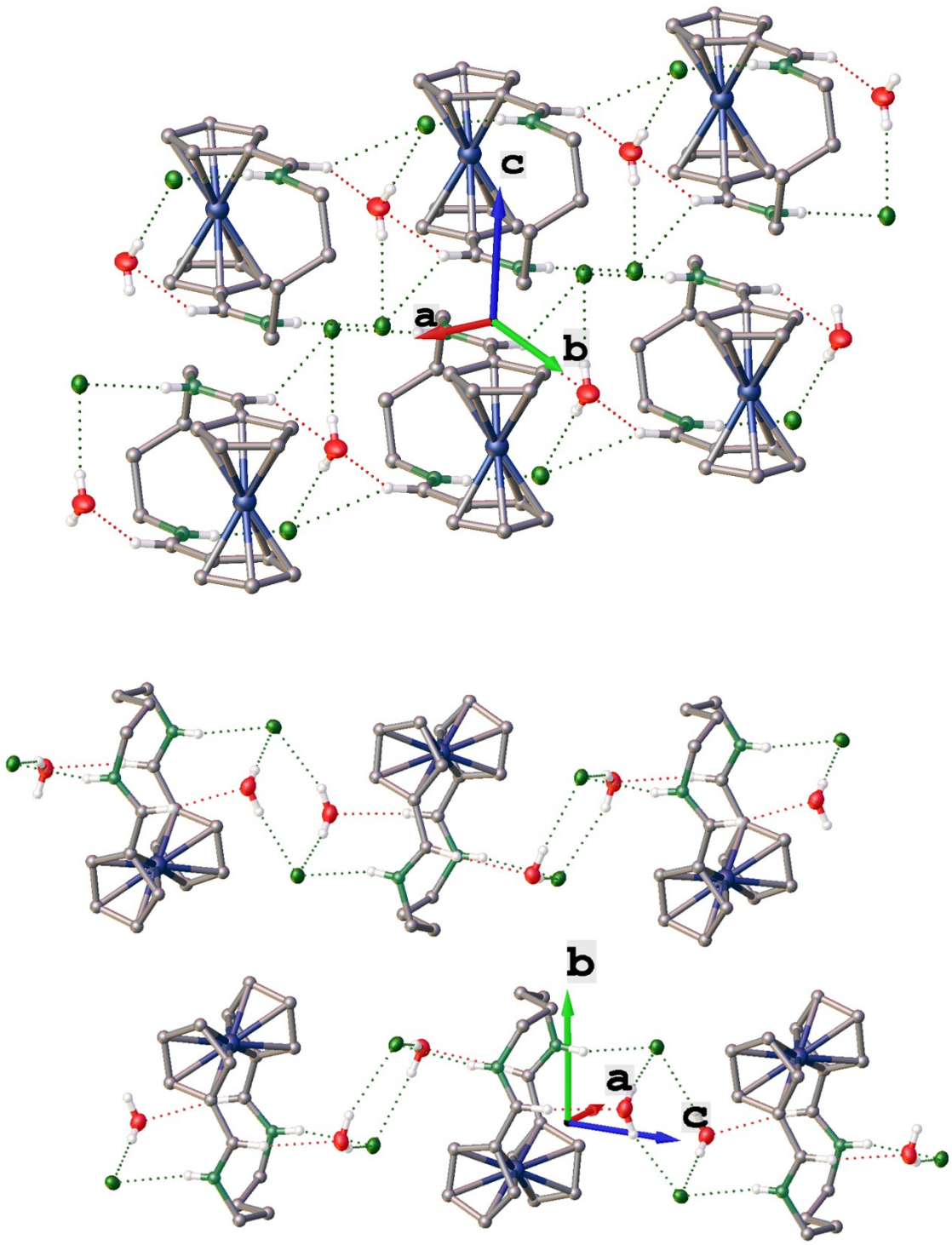

Figure S32. Packing of [H_2-**2b**]Cl_2·2H_2O in the crystal; Modification crystallised in the space group $P2_1/n$ (top) and in C2/c (bottom).

To visualise intermolecular interactions in the crystal, we generated Hirshfeld surfaces[8] from the single crystal X-ray data. Figure S33a shows a combined Hirshfeld surface for all ions in the crystal. Figure S33b shows an individual Hirshfeld surface generated only for the Zundel and chloride ions.

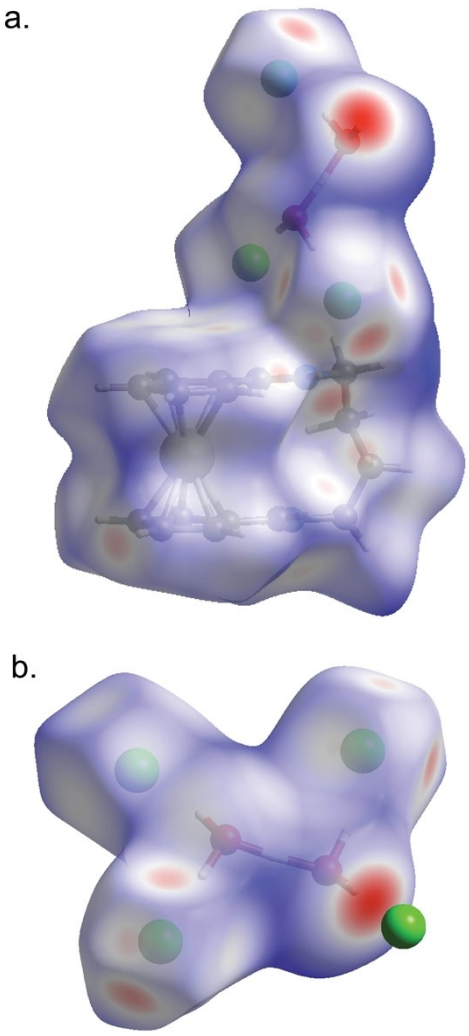

Figure S33. Hirshfeld surfaces of [H_2-**2b**]Cl_2·(H_5O_2)Cl (a) and the individual Zundel ion (b), generated with CrystalExplorer.[9]

A Hirshfeld surface is a 3D surface surrounding a molecule in a crystal lattice that defines the region where the electron density of the molecule dominates over that of neighbouring molecules. White areas indicate distances between atoms of the members of the surface to the next outside atom equal to the sum of their van der Waals distances. Blue areas are longer while red areas are

shorter than the sum of their van der Waals distances. Therefore, when analysing the Hirshfeld surfaces, more intense red areas indicate closer contacts to neighbouring molecules in the crystal lattice. The surfaces further confirm that the Zundel cation is stabilised by the chloride ions, which in turn are held in place by a network of hydrogen bonds with the ruthenocenophane dication.

The ruthenocenophanes $[H_2$-**2b**$]^{2+}$ and **3b** experience a mild tilt (*a*) of the Cp-ligands (Table S4). Compound $[H_2$-**2b**$]Cl_2 \cdot 2H_2O$ in $P2_1/n$ is tilted most with 4.94(7)°, while the polymorph in C2/c experiences a slightly lower tilt of 3.98(5)°, followed by $[H_2$-**2b**$]Cl_2 \bullet (H_5O_2)Cl$ and **3b**. The direction of this tilt is away from the eight-atomic handle to accommodate it. The handle furthermore induces a twist (*b*). The values *b* are the averages for all five Cp-C atoms of one Cp-ring to the closest C atom of the complementary Cp-ring bound to the same ruthenium atom. For the three different examples of the dications $[H_2$-**2b**$]^{2+}$, this twist varies from 19 to 30°, and for **3b**, it is 10°. The smaller twist in **3b** may be explained by the bulk of the attached Pd complexes, as these align as far away as possible from each other.

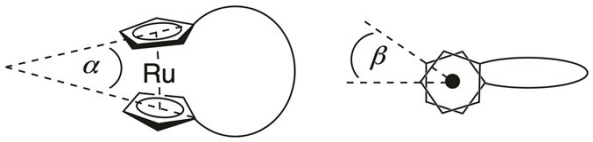

Table S4. Important angles (in °) of the ruthenocenophanes.

Compound	Tilt angle α	Twist angle β
$[H_2$-**2b**$]Cl_2 \cdot (H_5O_2)Cl$	3.67(5)	19.44
$[H_2$-**2b**$]Cl_2 \cdot 2H_2O$ / [C2/c]	3.98(5)	33.06
$[H_2$-**2b**$]Cl_2 \cdot 2H_2O$ / $[P2_1/n]$	4.94(7)	30.48
3b	1.99(8)	10.2

For **2a**, the C=N bond lengths vary from 1.265(6)–1.271(6) Å for the two non-disordered structures containing dichloromethane and water as co-solvates. Upon formation of $[H_2$-**2b**$]^{2+}$, the C=N bond lengths become slightly elongated (>1.280 Å). After coordination to Pd, the lengths vary from 1.266(8)–1.278(5) Å for **3a** and **3b**, indicating that the coordination does not significantly affect these bond lengths. Most Pd–N bonds are similar for both compounds, while one bond in **3a** is slightly longer (2.123(5) Å), which is most likely due to the proximity of two acetonitrile solvate molecules.

Table S5. Important bond lengths (in Å) of the macrocycle **2a**, the ruthenocenophane dications $[H_2$-**2b**$]^{2+}$ and the Pd adducts **3a**/**3b**.

Compound	C=N	Pd-N	Pd-C
2a·DCM	1.265(6), 1.268(7), 1.271(6), 1.271(7)	-	-
2a·H2O [a]	1.271(2), 1.271(2)	-	-
$[H_2$-**2b**$]Cl_2\cdot(H_5O_2)Cl$	1280(2), 1282(2)	-	-
$[H_2$-**2b**$]Cl_2\cdot 2H_2O$ [C2/c] [a]	1.285(2)	-	-
$[H_2$-**2b**$]Cl_2\cdot H_2O$ [$P2_1/n$]	1.284(2), 1.287(4)	-	-
3a [a]	1.266(8), 1.274(8)	2.085(5) 2.123(5)	1.965(7) 1.973(7)
3b	1.271(5), 1.278(5)	2.073(3) 2.076(3)	1.974(3) 1.959(3)

[a] The asymmetric unit contains half a molecule.

4. Computational Details

All calculations were performed using Gaussian 16 (G16).[10] Geometry optimisations of **2a** and **2b** were performed using four different functionals, B3LYP, B3LYP-D3, M06, and ωB97X-D, in the gas phase. The geometries of **2a** and **2b** were also optimised with the M06 functional, including the polarizable continuum SMD solvation model for chloroform. All geometry optimisations were carried out using the def2-SVP basis set. Frequency calculations were performed on the optimised structures at the same level of theory to confirm that the obtained structures correspond to minima and to derive thermal corrections to the free energy ΔG_{corr}. These corrections were recalculated at the selected temperatures (248.15 K or 323.15 K) and the condensed-phase standard state (1 M)[11] using Grimme's quasi-rigid rotor-harmonic oscillator approximation,[12] as implemented in the Goodvibes program.[13] A lower frequency cutoff of 50 cm^{-1} was applied, in line with recent recommendations,[14] instead of the standard 100 cm^{-1}. A vibrational scale factor of 1.0 was used in all cases. Single-point energy calculations E^{gas} and E^{solv} were conducted respectively at the DFT/def2-TZVPP and SMD($CHCl_3$)-DFT/def2-TZVPP levels using the optimised DFT/def2-SVP geometries for the four aforementioned DFT functionals. To ensure accurate geometries and energies, electronic structure calculations systematically employed tightened SCF convergence (10^{-8} atomic units), the "tight" optimisation keyword in Gaussian 16 (which tightens force and step-size convergence thresholds), and the "UltraFine" integration grid (99 radial shells and 590 angular points per shell). The Cartesian coordinates of the optimised structures are provided in a supplementary .xyz file.

To dissect the contributions of solvation, electronic energy, and thermal corrections to the free energy change ΔG_T for the transformation of **2a** to **2b**, we use the

thermodynamic cycle depicted in Scheme S3. This approach allows us to separate the gas phase and solvation components, providing a detailled understanding of the reaction energetics.

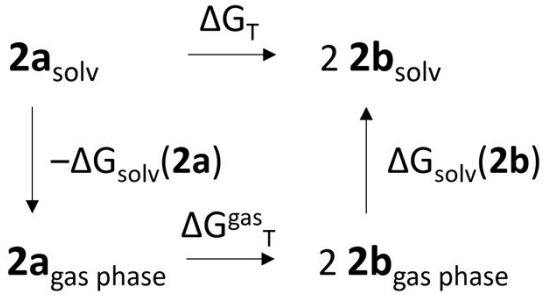

Scheme S3. Thermodynamic cycle for the transformation between **2a** and **2b**.

The free energy change ΔG_T is thus obtained by the following equation :

$\Delta G_T = 2\ \Delta G_{solv}(\mathbf{2b}) - \Delta G_{solv}(\mathbf{2a}) + \Delta G^{gas}{}_T$

Here, the solvation free energy difference $\Delta\Delta G_{solv}$ is defined as :

$$\Delta\Delta G_{solv} = 2\ \Delta G_{solv}(\mathbf{2b}) - \Delta G_{solv}(\mathbf{2a})$$
$$= 2\ [E^{solv}(\mathbf{2b}) - E^{gas}(\mathbf{2b})] - [E^{solv}(\mathbf{2a}) - E^{gas}(\mathbf{2a})]$$

E^{solv} and E^{gas} denote the electronic energies in the solvated and gas phases, respectively.

The gas phase free energy change $\Delta G^{gas}{}_T$ at temperature T is expressed as:

$$\Delta G^{gas}{}_T = 2\ G^{gas}{}_T(\mathbf{2b}) - G^{gas}{}_T(\mathbf{2a})$$
$$= 2\ [E^{gas}(\mathbf{2b}) + \Delta G^{T}{}_{corr}(\mathbf{2b})] - [E^{gas}(\mathbf{2a}) + \Delta G^{T}{}_{corr}(\mathbf{2a})]$$
$$= 2\ E^{gas}(\mathbf{2b}) - E^{gas}(\mathbf{2a}) + 2\ \Delta G^{T}{}_{corr}(\mathbf{2b}) - \Delta G^{T}{}_{corr}(\mathbf{2a})$$

We define the electronic energy difference in the gas phase (ΔE) and the difference in thermal corrections (including enthalpic and entropic contributions) at temperature T ($\Delta\Delta G_{corr}(T)$) as :

$\Delta E = 2\ E^{gas}(\mathbf{2b}) - E^{gas}(\mathbf{2a})$

and $\Delta\Delta G_{corr}(T) = 2\ \Delta G^{T}{}_{corr}(\mathbf{2b}) - \Delta G^{T}{}_{corr}(\mathbf{2a})$

Combining these terms, we obtain the final expression for the free energy change :

$\Delta G_T = \Delta E + \Delta\Delta G_{corr}(T) + \Delta\Delta G_{solv}$

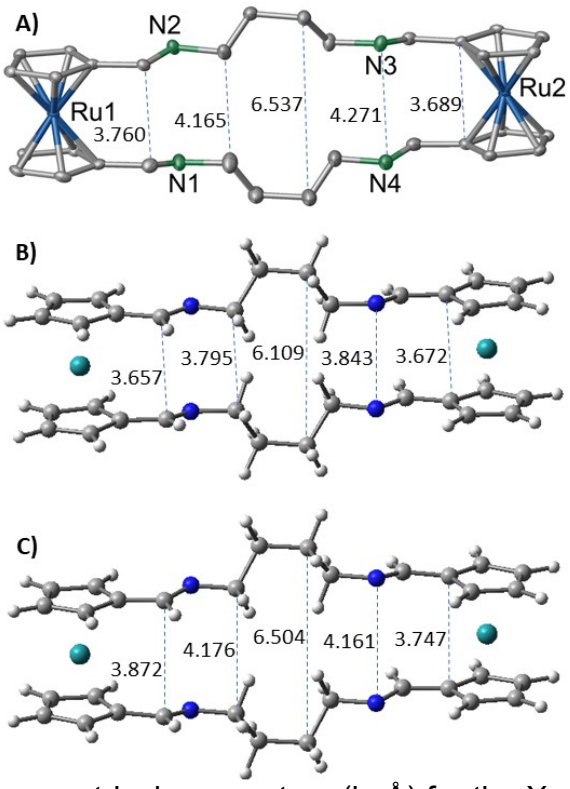

Figure S34. Selected geometrical parameters (in Å) for the X-ray experimental structure of **2a**·DCM (average values) (A) and theoretical structure of **2a** at the B3LYP-D3/def2-SVP (B) and B3LYP/def2-SVP (C) levels.

Table S6. Absolute electronic energies and thermal corrections (in a.u.) for **2a** and **2b**.

	DFT	E DFT/ def2-SVP	qh-G(248)[a] DFT/ def2-SVP	qh-G(323)[a] DFT/ def2-SVP	E DFT/ def2-TZVPP[b]	E SMD(CHCl3)-DFT/ def2-TZVPP[b]
2a	B3LYP	-1648.913608	-1648.350581	-1648.373548	-1650.564413	-1650.613644
2a	B3LYP-D3	-1648.995094	-1648.430409	-1648.453154	-1650.645483	-1650.693731 -1650.694802[c]
2a	M06	-1647.747314	-1647.186930	-1647.209744	-1649.403317	-1649.450442
2a	M06[d]	-1647.793013				
2a	ωB97X-D	-1648.48645	-1647.9121	-1647.93408	-1650.10591	-1650.15517
2b	B3LYP	-824.451210	-824.176585	-824.190148	-825.275992	-825.299965
2b	B3LYP-D3	-824.490083	-824.215358	-824.228904	-825.314923	-825.338808 -825.337599[c]
2b	M06	-823.868903	-823.595840	-823.609375	-824.696593	-824.720101
2b	ωB97X-D	-824.236363	-823.957141	-823.970501	-825.045305	-825.069675

[a] Quasi-harmonic corrected free energy obtained at the DFT/def2-SVP level, calculated at 248.15 or 323.15 K with a vibrational scale factor of 1.0 and the condensed-phase standard state (1 M) using Grimme's quasi-rigid rotor-harmonic oscillator approximation for low-frequency vibration (cut-off at 50 cm^{-1}); [b] Single-point energies computed at the DFT/def2-SVP geometries; [c] Energies computed at the SMD(methanol)-B3LYP-D3/def2-TZVPP level; [d] Geometry optimisation at the SMD(CHCl3)-M06/def2-SVP level.

5. References

1. H. V. Huynh, Y. Han, J. H. H. Ho and G. K. Tan, Palladium(II) Complexes of a Sterically Bulky, Benzannulated N-Heterocyclic Carbene with Unusual Intramolecular C−H···Pd and Ccarbene···Br Interactions and Their Catalytic Activities, *Organometallics*, 2006, **25**, 3267-3274.
2. G. R. Fulmer, A. J. M. Miller, N. H. Sherden, H. E. Gottlieb, A. Nudelman, B. M. Stoltz, J. E. Bercaw and K. I. Goldberg, NMR Chemical Shifts of Trace Impurities: Common Laboratory Solvents, Organics, and Gases in Deuterated Solvents Relevant to the Organometallic Chemist, *Organometallics*, 2010, **29**, 2176-2179.
3. L. Bednarik and E. Neuse, Lithiierung und iodierung von ruthenocen, *J. Organomet. Chem.*, 1979, **168**, C8-C12.
4. R. Sanders and U. T. Mueller-Westerhoff, The lithiation of ferrocene and ruthenocene: a retraction and an improvement, *J. Organomet. Chem.*, 1996, **512**, 219-224.
5. M. Roemer and C. A. Nijhuis, Syntheses and purification of the versatile synthons iodoferrocene and 1,1’-diiodoferrocene, *Dalton Trans.*, 2014, **43**, 11815-11818.
6. A. A. Hoser, Ł. Dobrzycki, M. J. Gutmann and K. Woźniak, Charge Densities of Two Polymorphs of Hydrated 1,8-Bis(dimethylamino)naphthalene Hydrochloride – Similarities and Differences, *Cryst. Grow. Des.*, 2010, **10**, 5092-5104.
7. K. Molčanov, J. Stare, M. V. Vener, B. Kojić-Prodić, G. Mali, J. Grdadolnik and V. Mohaček-Gročev, Nitranilic acid hexahydrate, a novel benchmark system of the Zundel cation in an intrinsically asymmetric environment: spectroscopic

features and hydrogen bond dynamics characterised by experimental and theoretical methods, *Phys. Chem. Chem. Phys.*, 2014, **16**, 998-1007.

8. M. A. Spackman and D. Jayatilaka, Hirshfeld surface analysis, *CrystEngComm*, 2009, **11**, 19-32.

9. P. R. Spackman, M. J. Turner, J. J. McKinnon, S. K. Wolff, D. J. Grimwood, D. Jayatilaka and M. A. Spackman, CrystalExplorer: a program for Hirshfeld surface analysis, visualization and quantitative analysis of molecular crystals, *J. Appl. Cryst.*, 2021, **54**, 1006-1011.

10. M. J. Frisch, G. W. Trucks, H. B. Schlegel, G. E. Scuseria, M. A. Robb, J. R. Cheeseman, G. Scalmani, V. Barone, G. A. Petersson, H. Nakatsuji, X. Li, M. Caricato, A. V. Marenich, J. Bloino, B. G. Janesko, R. Gomperts, B. Mennucci, H. P. Hratchian, J. V. Ortiz, A. F. Izmaylov, J. L. Sonnenberg, Williams, F. Ding, F. Lipparini, F. Egidi, J. Goings, B. Peng, A. Petrone, T. Henderson, D. Ranasinghe, V. G. Zakrzewski, J. Gao, N. Rega, G. Zheng, W. Liang, M. Hada, M. Ehara, K. Toyota, R. Fukuda, J. Hasegawa, M. Ishida, T. Nakajima, Y. Honda, O. Kitao, H. Nakai, T. Vreven, K. Throssell, J. A. Montgomery Jr., J. E. Peralta, F. Ogliaro, M. J. Bearpark, J. J. Heyd, E. N. Brothers, K. N. Kudin, V. N. Staroverov, T. A. Keith, R. Kobayashi, J. Normand, K. Raghavachari, A. P. Rendell, J. C. Burant, S. S. Iyengar, J. Tomasi, M. Cossi, J. M. Millam, M. Klene, C. Adamo, R. Cammi, J. W. Ochterski, R. L. Martin, K. Morokuma, O. Farkas, J. B. Foresman and D. J. Fox, *Gaussian 16 Rev. C.01*, 2016.

11. J. N. Harvey, F. Himo, F. Maseras and L. Perrin, Scope and Challenge of Computational Methods for Studying Mechanism and Reactivity in Homogeneous Catalysis, *ACS Catal.*, 2019, **9**, 6803-6813.

12. S. Grimme, Supramolecular Binding Thermodynamics by Dispersion-Corrected Density Functional Theory, *Chem. Eur. J.*, 2012, **18**, 9955-9964.

13. A.-R. J. Luchini G, Funes-Ardoiz I and Paton RS, GoodVibes: automated thermochemistry for heterogeneous computational chemistry data, *F1000Research*, 2020, **9**.

14. N. Tarannam, N. Alassad, N. G. Lemcoff and S. Kozuch, Right Answer for the Right Reason? Benchmarking Protocols and Pitfalls on a Ru-Metathesis Example, *J. Chem. Theory Comput.*, 2023, **19**, 5024-5035.

6. High Resolution Mass Spectra

Meas. m/z	#	Formula	Calc. Mass	Err [ppm]
681.1113	1	C32 H37 N4 [102Ru]2	681.1118	0.73

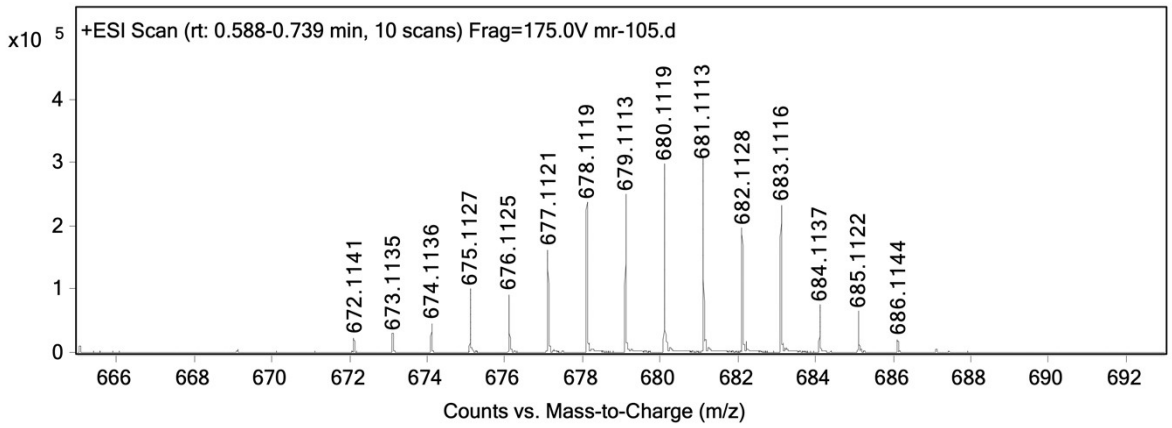

Meas. m/z	#	Formula	Calc. Mass	Err [ppm]
341.0592	1	C16 H19 N2 [102Ru]	341.0591	0.29

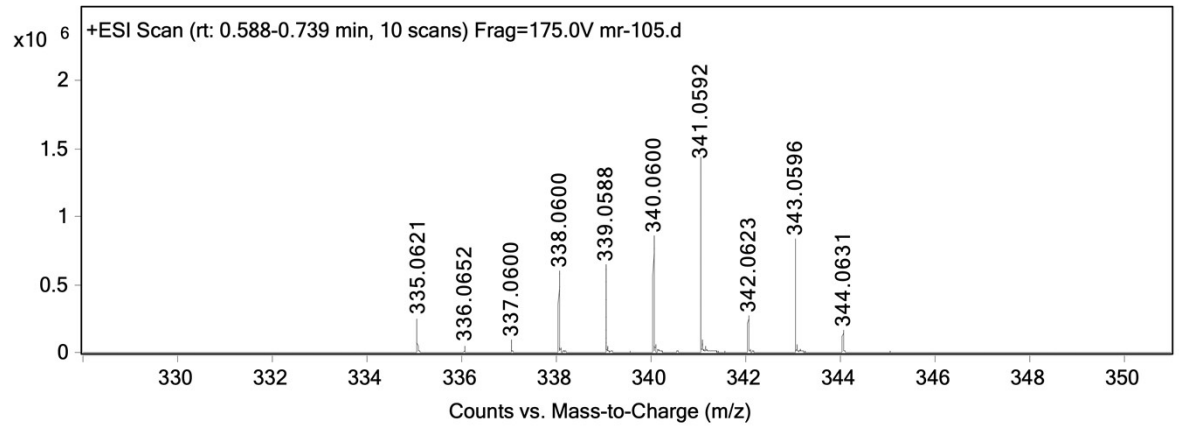

Meas. m/z	#	Formula	Calc. Mass	Err [ppm]
371.1059	1	C18 H25 N2 Ru	371.1061	0.54

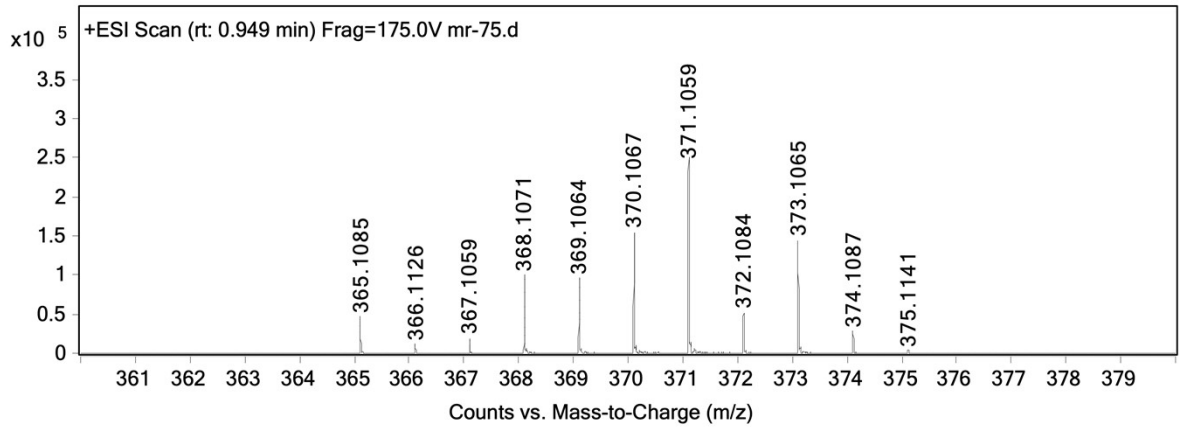

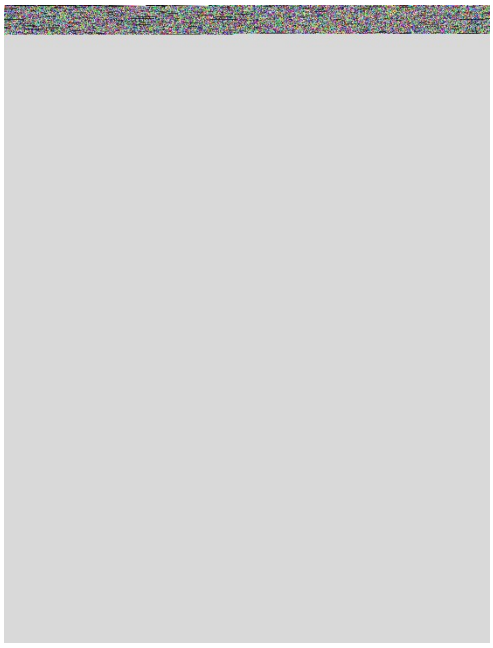

Meas. m/z	#	Formula	Calc. Mass	Err [ppm]
2464.7356	1	C84 H108 Br7 N12 [106Pd]4 [102Ru]2	2464.7349	0.28

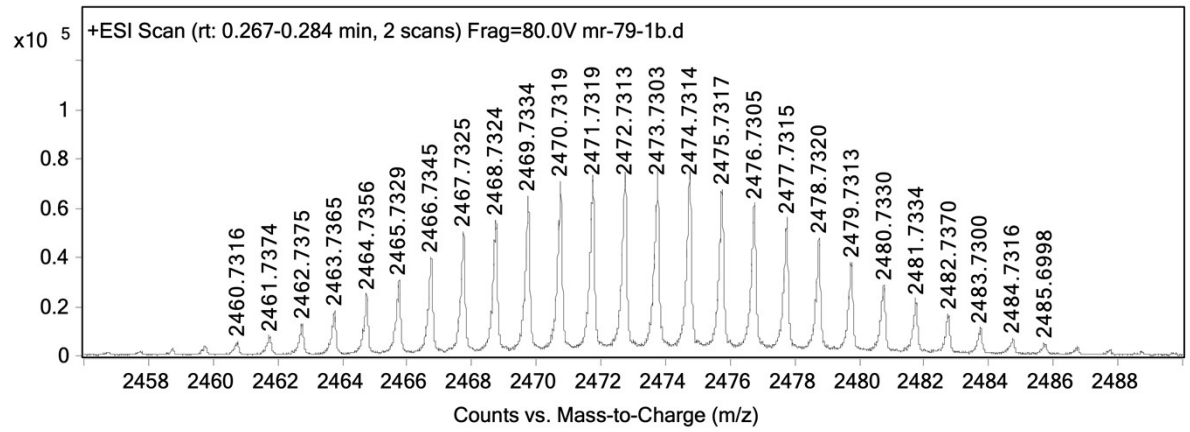

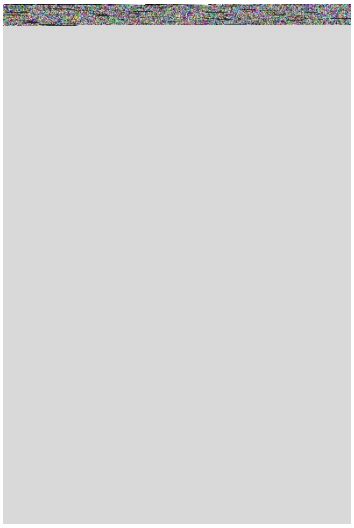

Meas. m/z	#	Formula	Calc. Mass	Err [ppm]
1192.9079	1	C42 H54 Br3 N6 [106Pd]2 [102Ru]	1192.9080	0.08

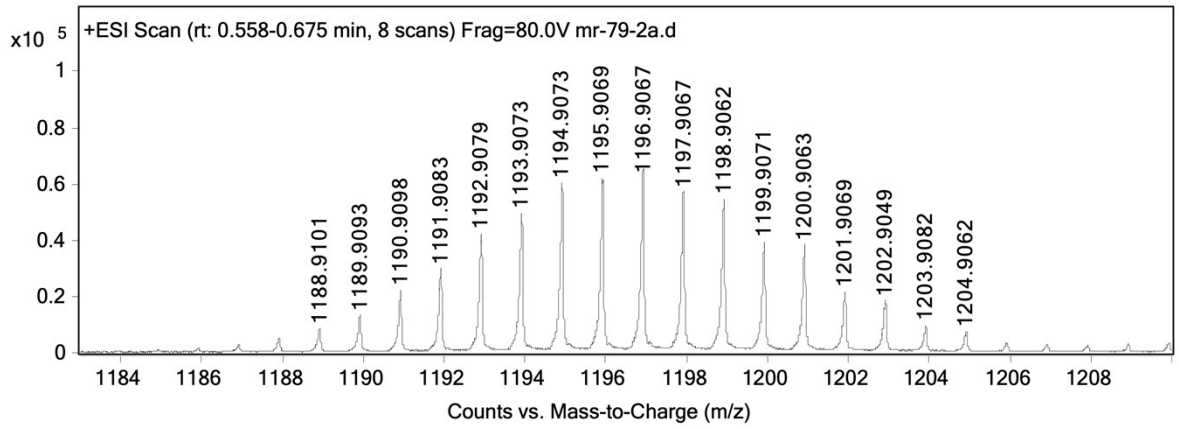

7. NMR Spectra

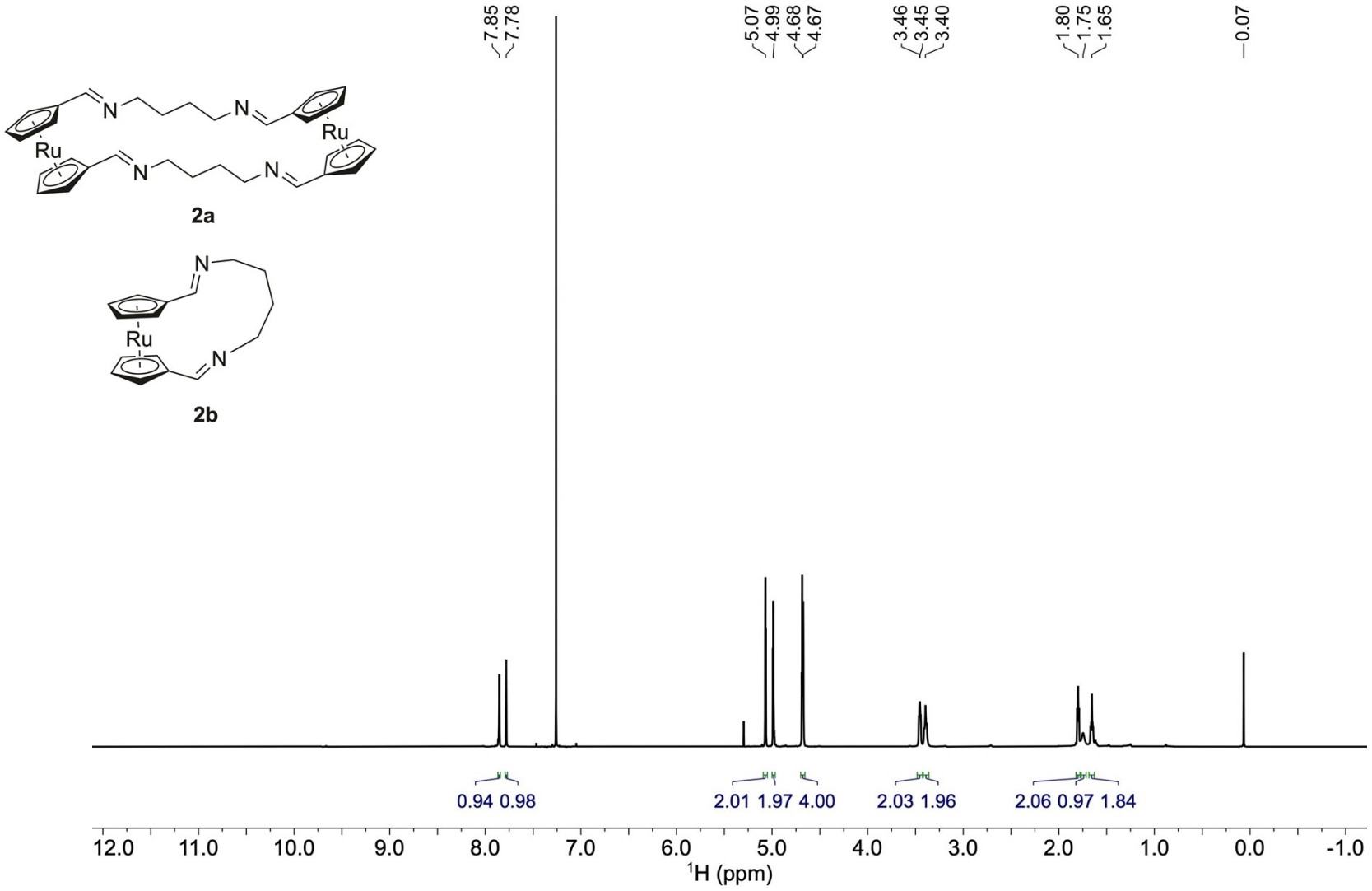

2a

2b

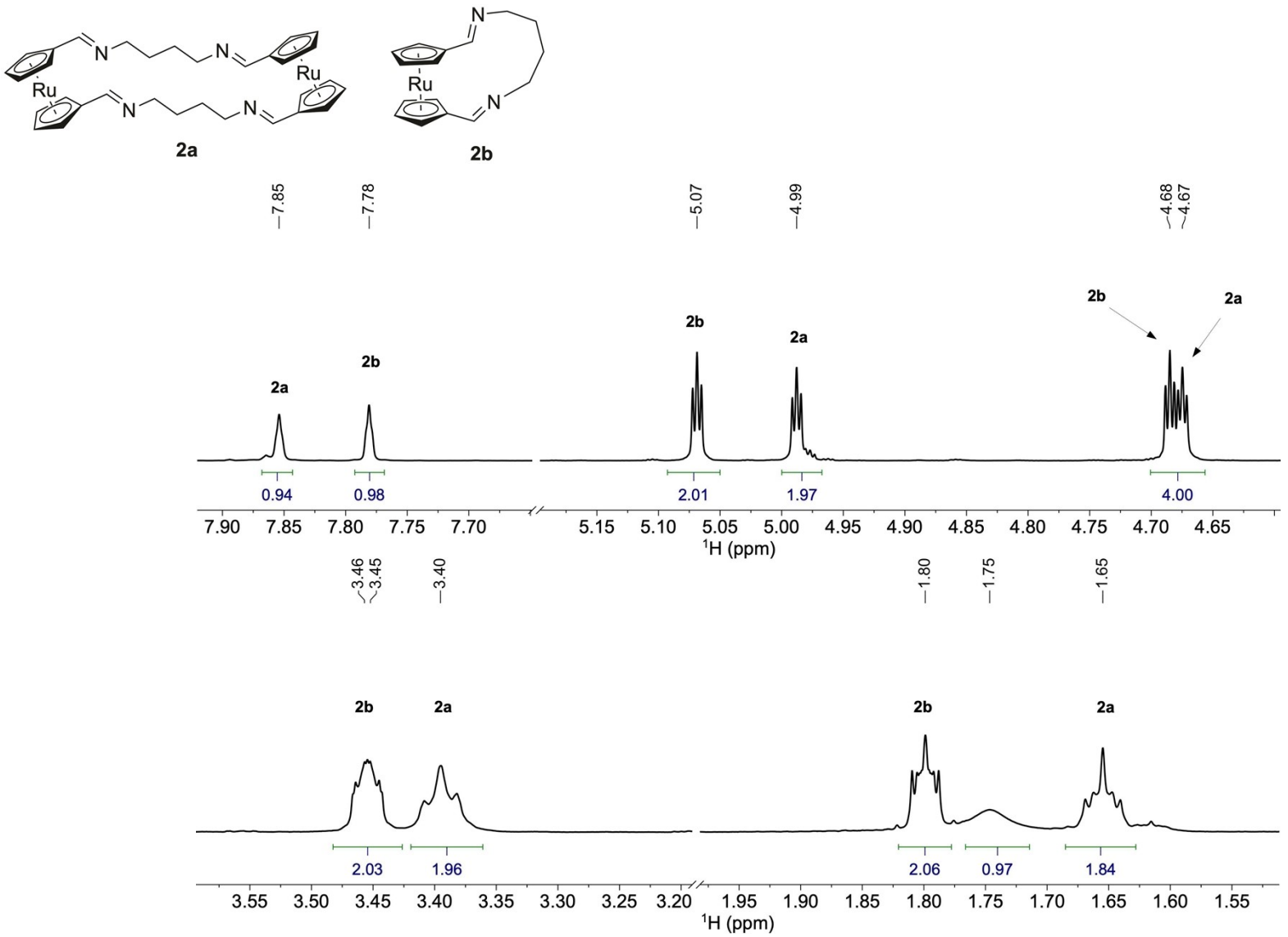
2a
2b
7.85
7.78
5.07
4.99
4.68
4.67
2a
2b
2b
2a
2b
2a
0.94
0.98
2.01
1.97
4.00
7.90 7.85 7.80 7.75 7.70
5.15 5.10 5.05 5.00 4.95 4.90 4.85 4.80 4.75 4.70 4.65
1H (ppm)
3.46
3.45
3.40
1.80
1.75
1.65
2b
2a
2b
2a
2.03
1.96
2.06
0.97
1.84
3.55 3.50 3.45 3.40 3.35 3.30 3.25 3.20
1.95 1.90 1.85 1.80 1.75 1.70 1.65 1.60 1.55
1H (ppm)

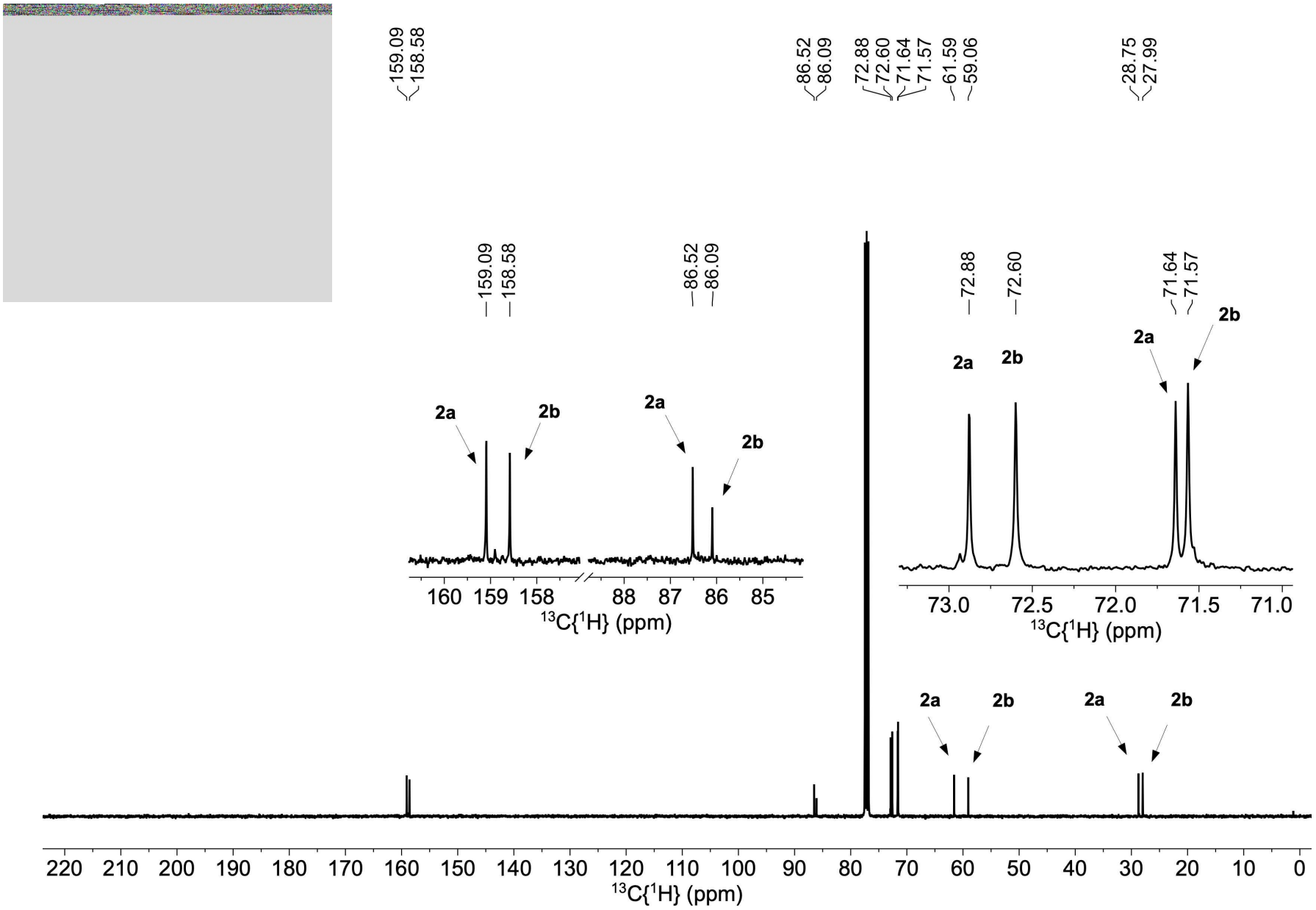
159.09
158.58
86.52
86.09
72.88
72.60
71.64
71.57
61.59
59.06
28.75
27.99
2a
2b
220 210 200 190 180 170 160 150 140 130 120 110 100 90 80 70 60 50 40 30 20 10 0
$^{13}C\{^{1}H\}$ (ppm)
160 159 158
88 87 86 85
73.0 72.5 72.0 71.5 71.0

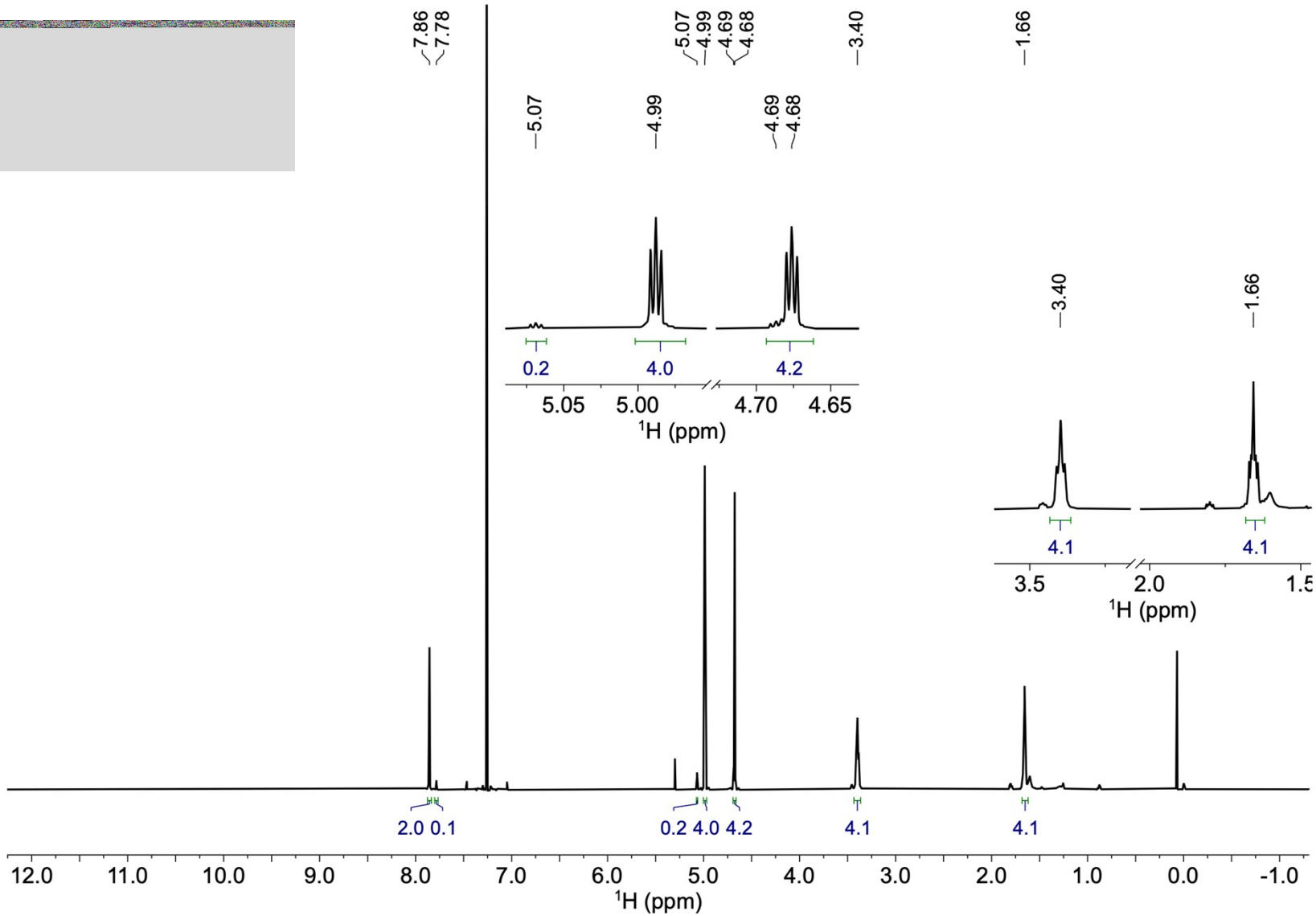
7.86
7.78
5.07
4.99
4.69
4.68
3.40
1.66
0.2
4.0
4.2
5.05
5.00
4.70
4.65
^{1}H (ppm)
4.1
4.1
3.5
2.0
^{1}H (ppm)
2.0 0.1
0.2 4.0 4.2
4.1
4.1
12.0
11.0
10.0
9.0
8.0
7.0
6.0
5.0
4.0
3.0
2.0
1.0
0.0
-1.0
^{1}H (ppm)

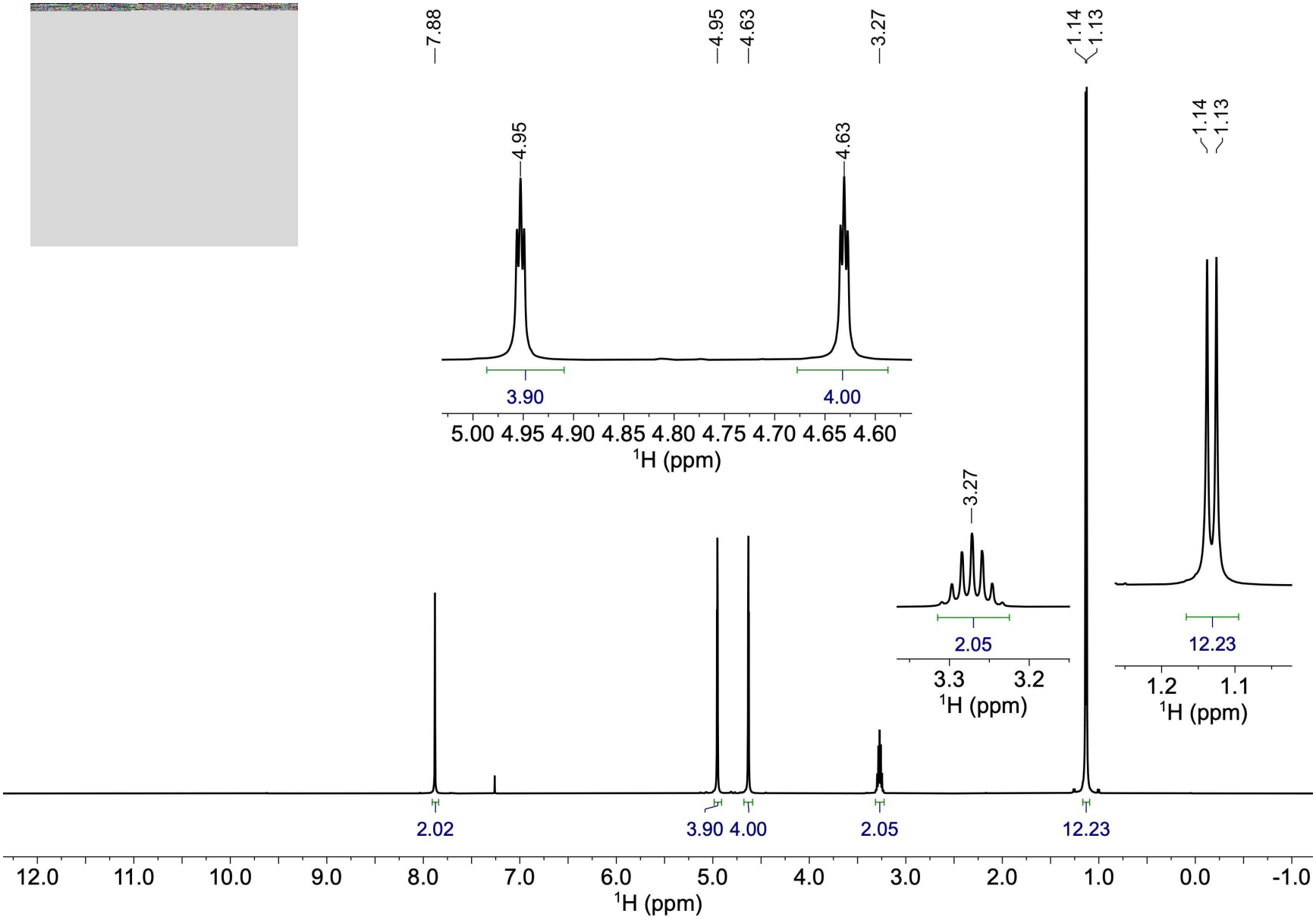
7.88
4.95
4.63
3.27
1.14
1.13
3.90
4.00
5.00 4.95 4.90 4.85 4.80 4.75 4.70 4.65 4.60
1H (ppm)
2.05
3.3 3.2
1H (ppm)
12.23
1.2 1.1
1H (ppm)
2.02
3.90 4.00
2.05
12.23
12.0 11.0 10.0 9.0 8.0 7.0 6.0 5.0 4.0 3.0 2.0 1.0 0.0 -1.0
1H (ppm)

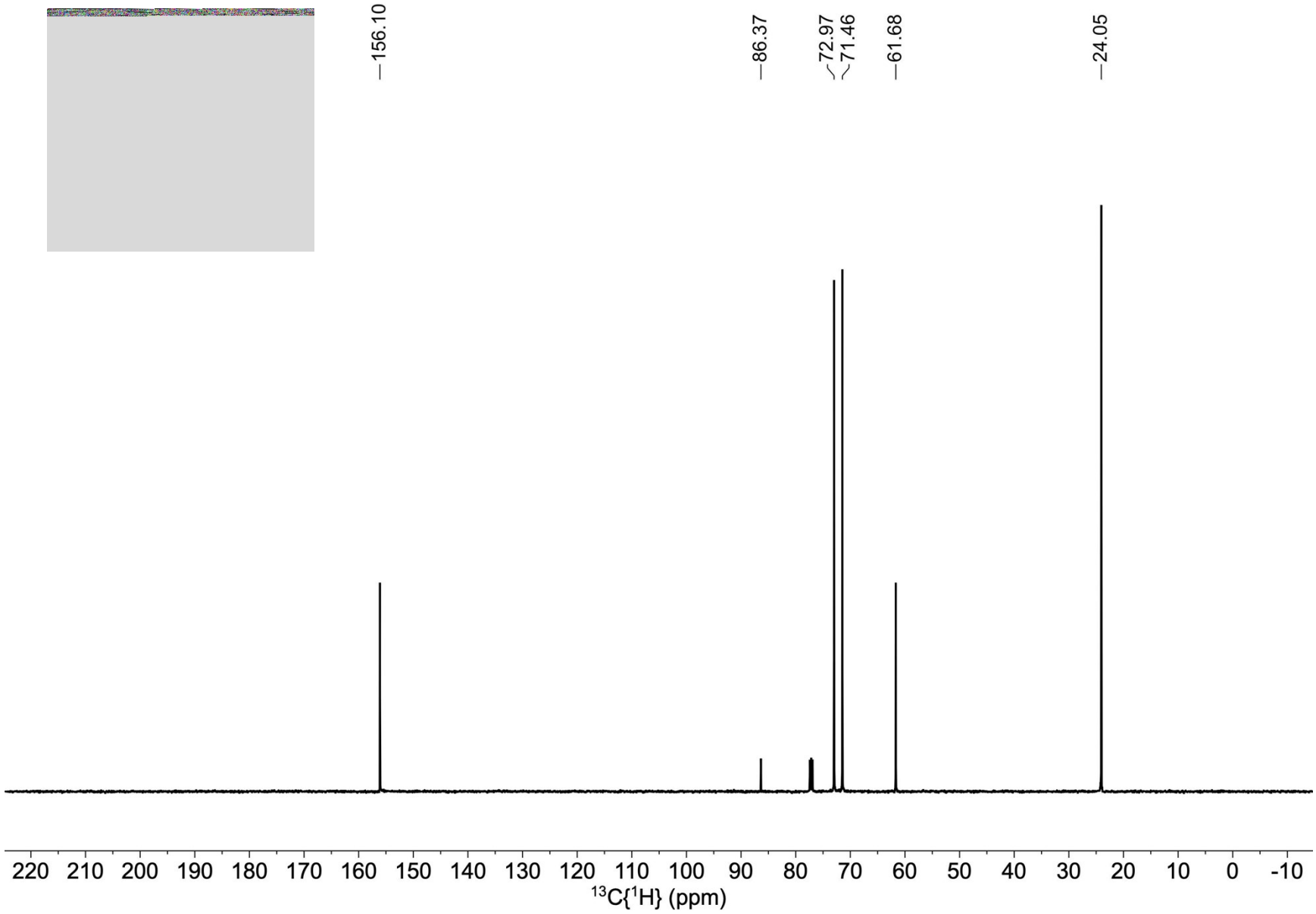
156.10
86.37
72.97
71.46
61.68
24.05
220 210 200 190 180 170 160 150 140 130 120 110 100 90 80 70 60 50 40 30 20 10 0 -10
$^{13}C\{^{1}H\}$ (ppm)

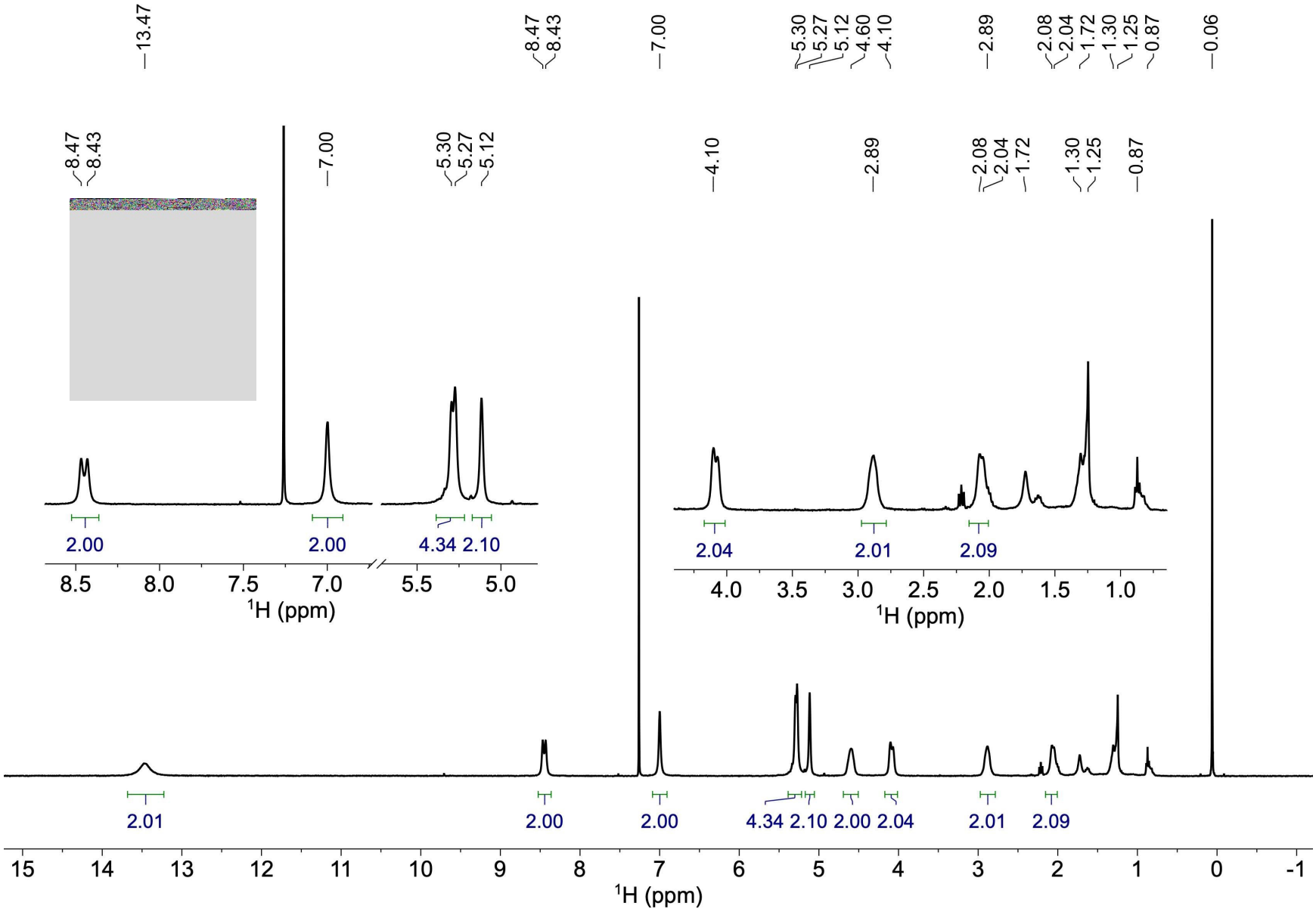
13.47
8.47
8.43
7.00
5.30
5.27
5.12
4.60
4.10
2.89
2.08
2.04
1.72
1.30
1.25
0.87
0.06
2.01
2.00
2.00
4.34
2.10
2.00
2.04
2.01
2.09
15 14 13 12 11 10 9 8 7 6 5 4 3 2 1 0 -1
1H (ppm)
2.00
2.00
4.34
2.10
8.5 8.0 7.5 7.0 5.5 5.0
1H (ppm)
2.04
2.01
2.09
4.0 3.5 3.0 2.5 2.0 1.5 1.0
1H (ppm)

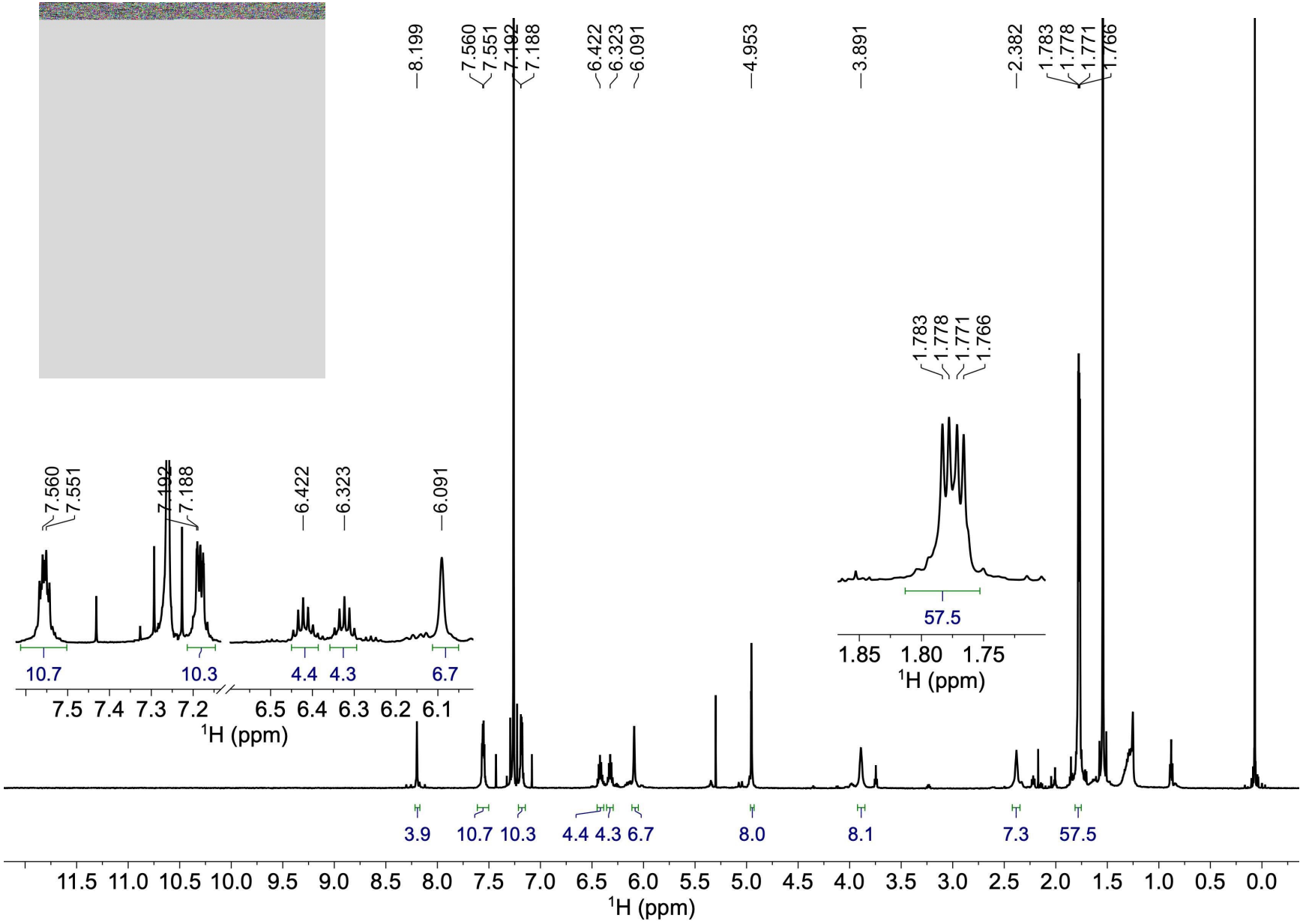
8.199
7.560
7.551
7.192
7.188
6.422
6.323
6.091
4.953
3.891
2.382
1.783
1.778
1.771
1.766
3.9
10.7
10.3
4.4
4.3
6.7
8.0
8.1
7.3
57.5
11.5 11.0 10.5 10.0 9.5 9.0 8.5 8.0 7.5 7.0 6.5 6.0 5.5 5.0 4.5 4.0 3.5 3.0 2.5 2.0 1.5 1.0 0.5 0.0
^{1}H (ppm)
10.7
10.3
4.4
4.3
6.7
7.5 7.4 7.3 7.2 6.5 6.4 6.3 6.2 6.1
^{1}H (ppm)
57.5
1.85 1.80 1.75
^{1}H (ppm)

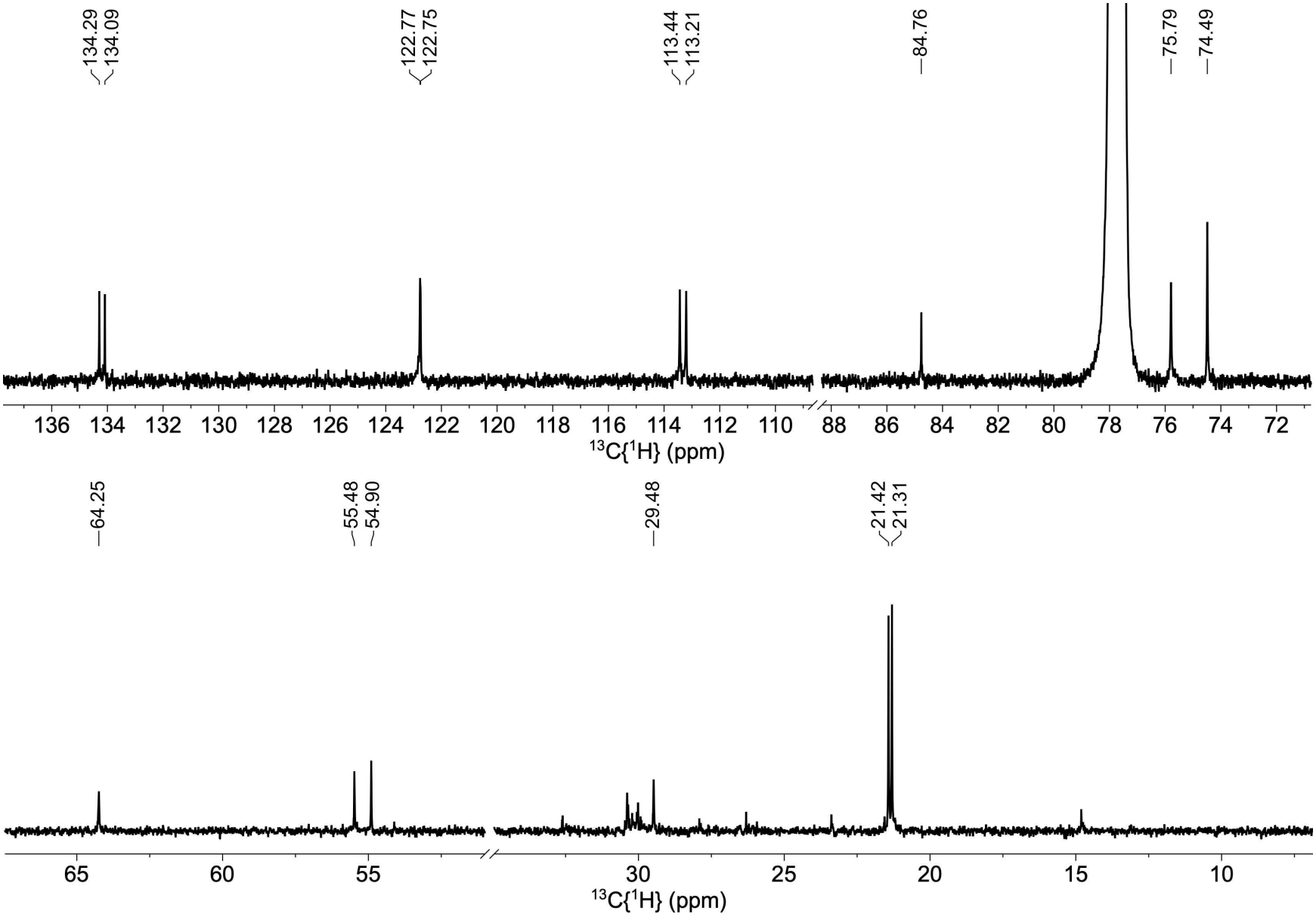
134.29
134.09
122.77
122.75
113.44
113.21
84.76
75.79
74.49
136 134 132 130 128 126 124 122 120 118 116 114 112 110 88 86 84 82 80 78 76 74 72
$^{13}C\{^{1}H\}$ (ppm)
64.25
55.48
54.90
29.48
21.42
21.31
65 60 55 30 25 20 15 10
$^{13}C\{^{1}H\}$ (ppm)